Journal of Magnetic Resonance 241 (2014) 155–169

Contents lists available at ScienceDirect

Journal of Magnetic Resonance

journal homepage: www.elsevier.com/locate/jmr

Proton-decoupled CPMG: A better experiment for measuring ^{15}N R_2 relaxation in disordered proteins

Tairan Yuwen, Nikolai R. Skrynnikov *

Department of Chemistry, Purdue University, West Lafayette, IN 47907, USA

ARTICLE INFO

Article history:
Received 27 June 2013
Revised 15 August 2013
Available online 23 August 2013

Keywords:
^{15}N relaxation
Intrinsically disordered proteins
CPMG experiment
Spin-lock experiment
Ubiquitin
α-Spectrin SH3 domain
Solvent exchange
Backbone dynamics
Arginine side-chain dynamics
Spin simulations

ABSTRACT

^{15}N R_2 relaxation is one of the most informative experiments for characterization of intrinsically disordered proteins (IDPs). Small changes in nitrogen R_2 rates are often used to determine how IDPs respond to various biologically relevant perturbations such as point mutations, posttranslational modifications and weak ligand interactions. However collecting high-quality ^{15}N relaxation data can be difficult. Of necessity, the samples of IDPs are often prepared with low protein concentration and the measurement time can be limited because of rapid sample degradation. Furthermore, due to hardware limitations standard experiments such as ^{15}N spin-lock and CPMG can sample the relaxation decay only to ca. 150 ms. This is much shorter than ^{15}N T_2 times in disordered proteins at or near physiological temperature. As a result, the sampling of relaxation decay profiles in these experiments is suboptimal, which further lowers the precision of the measurements.

Here we report a new implementation of the proton-decoupled (PD) CPMG experiment which allows one to sample ^{15}N R_2 relaxation decay up to ca. 0.5–1 s. The new experiment has been validated through comparison with the well-established spin-lock measurement. Using dilute samples of denatured ubiquitin, we have demonstrated that PD-CPMG produces up to 3-fold improvement in the precision of the data. It is expected that for intrinsically disordered proteins the gains may be even more substantial. We have also shown that this sequence has a number of favorable properties: (i) the spectra are recorded with narrow linewidth in nitrogen dimension; (ii) ^{15}N offset correction is small and easy to calculate; (iii) the experiment is immune to various spurious effects arising from solvent exchange; (iv) the results are stable with respect to pulse miscalibration and *rf* field inhomogeneity; (v) with minimal change, the pulse sequence can also be used to measure R_2 relaxation of $^{15}N^{\varepsilon}$ spins in arginine side chains. We anticipate that the new experiment will be a valuable addition to the NMR toolbox for studies of IDPs.

1. Introduction

^{15}N relaxation measurement is one of the most useful NMR experiments – it is fast, reasonably simple to interpret, and immediately provides information on protein backbone flexibility. This information can be further used to characterize the role of motions (i.e. conformational entropy) in ligand binding [1,2], protein stability [3,4], allosteric regulation [5,6], etc.

The spin context of ^{15}N relaxation is fairly straightforward. It is normally assumed that nitrogen relaxation is driven by $^1H^N$–^{15}N dipolar interaction and, to a lesser degree, by ^{15}N CSA mechanism. Nevertheless, even in this sufficiently simple spin system there is room for uncertainty – the appropriate length of N–H bond was a subject of debate and the degree of anisotropy and site-to-site variation of the ^{15}N CSA tensors have also been widely discussed [7,8]. Furthermore, small and difficult-to-quantify R_{ex} contributions into ^{15}N R_2 appear to be more common than previously thought [9].

In addition to these fundamental sources of uncertainty, there are also a number of errors associated with specific measurement schemes that have been uncovered in recent years. For example, it has been found that frequent application of ^1H pulses during the spin-lock period with the intention to suppress dipolar-CSA cross-correlation may actually re-introduce the undesirable J-coupling evolution [10]. In $^1H^N$–^{15}N saturation-transfer NOE experiment it was found that the standard saturation sequence tends to create a number of unwanted spin modes [11]. The artefacts associated with solvent exchange were also recently exposed [12].

Finally, there are also uncertainties associated with the choice of the model. The most common approach is to choose from several versions of the model-free model which make different assumptions about the underlying dynamics – in particular, with regard to local motions on ~1 ns time scale [13–15]. While there are statistical criteria that guide this choice, it has been shown that the outcome is often influenced by the random noise-like errors

* Corresponding author.
E-mail address: nikolai@purdue.edu (N.R. Skrynnikov).

1090-7807/$ - see front matter © 2013 Elsevier Inc. All rights reserved.
http://dx.doi.org/10.1016/j.jmr.2013.08.008

and depends on availability of data measured at different magnetic fields [16–18]. An additional level of complexity is added by the protein's overall tumbling, which should be properly modeled using a fully asymmetric diffusion tensor [19–22].

With all of these sources of uncertainty combined, it is not surprising that ^{15}N-relaxation-derived motional parameters are not necessarily very accurate. Consider, for example, the well-studied model protein ubiquitin, where several groups independently measured and analyzed ^{15}N relaxation in solution [20,23–25]. The backbone order parameters reported in these studies differ significantly from each other: the *rms* deviations between the independently determined sets of S^2 are in the range from 0.02 to 0.07 and the correlation coefficients are in the range from 0.56 to 0.94.

In practice, however, the perceived lack of accuracy is not very important so long as most experimental studies focus on the difference in order parameters, ΔS^2, rather than the absolute values. It is reasonably safe to assume that systematic biases subtract out in calculating ΔS^2 and the result correctly represents changes in local dynamics. The examples include changes in order parameters in response to ligand binding, point mutations, various post-translational modifications, etc. [26–29]. Given that such changes are typically small, on the order of 0.05 or less, the primary concern is the *precision* of the data – i.e. it is important to ensure that small ΔS^2 values can be experimentally reproduced and quantitated in a reliable fashion.

These considerations are especially relevant for intrinsically disordered proteins (IDPs), which have emerged as the area of major biomedical interest [30]. IDPs do not lend themselves to the standard methods of structural characterization. Instead, the dynamics-oriented experiments play a prominent role. In particular, ^{15}N relaxation and paramagnetic relaxation enhancements (PREs) are arguably two most informative experiments in the field of intrinsically disordered proteins. At the same time, it is often considerably more difficult to achieve high precision in measuring ^{15}N relaxation rates in IDPs. Many disordered proteins are prone to aggregation which makes it necessary to work with low-concentration NMR samples, often in the range 10–100 μM, and/or collect the data over a short period of time to avoid sample degradation [31–33]. If the studies are conducted at or near physiological conditions (37 °C, pH 7.4), the quality of the already crowded spectra suffers from the line-broadening caused by solvent exchange, which further lowers the signal-to-noise ratio. Finally, there is one other issue that is concerned specifically with ^{15}N R_2 measurements as discussed below.

For disordered proteins at 37 °C the ^{15}N T_2 relaxation times are relatively long, on the order of 0.5–1.0 s. On the other hand, the length of the spin-lock period τ_{rel} in the standard $R_{1\rho}$ experiment does not exceed ca. 100–150 ms, as dictated by hardware limitations. It is clearly not possible to properly sample the magnetization decay curve over such a short interval of time. This situation is illustrated in Fig. 1a, which shows the $R_{1\rho}$ decay curve from residue L15 in a 100 μM sample of denatured ubiquitin at 37 °C. The expansion of this relaxation profile in Fig. 1b demonstrates the problem with such measurement – generally, when τ_{rel} is much shorter than T_2 the decay profile appears flat, which makes it difficult to accurately determine the relaxation rate constant. A rigorous treatment indicates that the best results are obtained when τ_{rel} is extended beyond T_2 [34].

The restrictions concerning the maximum length of τ_{rel} are ultimately due to low gyromagnetic ratio of nitrogen, $\omega_1 = -\gamma_N B_1$. In order to generate sufficiently strong ^{15}N *rf* field which is necessary to suppress the effect of $^1J_{NH}$ coupling, a very strong current should be applied to the transmitter coil. This pushes the probe to the limits of its performance. In the case of spin-lock measurements, the room-temperature probe can sustain 1.7 kHz nitrogen *rf* field for a period of time ca. 150 ms. In the case of R_2 CPMG measurements, the probe can withstand the pulse train with the repetition time of 1 ms for ca. 100 ms. For early-generation cryogenic probes the power limits are even more restrictive. Extending τ_{rel} beyond these limits can lead to excessive heating of the sample and cause probe arcing [35] which severely degrades the performance of the pulse sequence. In the worst-case scenario, the probe can be permanently damaged.

It appears that the latest-generation hardware and particularly new cryogenic probes should make it possible to run spin-lock experiment with long τ_{rel} [36]. Preliminary data obtained by Ban and Lee suggest that nitrogen *rf* field with the strength of 3 kHz can be maintained for 500 ms using reasonable duty cycle of 20% (personal communication). In these trial experiments *rf* power remains stable (i.e. there is no observable amplifier drooping) and *rf* coil experiences little or no heating. The sample heating is also modest, even for high-salt samples, which can be attributed to the improvements in probe head design. These favorable properties can potentially lead to a robust R_2 experiment well suited for application to samples of IDPs at or near physiological conditions. However, to the best of our knowledge, such strategy has never been tested experimentally. One should also bear in mind that the latest-generation hardware which is necessary for such measurements is available only to a handful of research groups.

The problem can also be managed without recourse to advanced hardware. For example, Palmer and co-workers demonstrated that $^1J_{NH}$ coupling can be suppressed by using relatively weak ^{15}N spin lock plus a small number of strategically placed ^{1}H pulses [37]. This experiment, however, is semi-selective – to collect a complete $R_{1\rho}$ dataset one needs to repeat the measurements several times using different ^{15}N carrier settings.

The alternative solution, which we pursue in this report, is to use ^{1}H decoupling to suppress $^1J_{NH}$. Because of the high gyromagnetic ratio of the proton, it is easy to generate a sufficiently strong *rf* field without overloading the probe. In the presence of proton decoupling, ^{15}N 180° pulses can be applied only infrequently (for the purpose of refocusing chemical shift evolution). Using this approach, τ_{rel} can be extended by at least a factor of 5 without risking adverse consequences to a probe.

A suitable pulse sequence, proton-decoupled CPMG (PD-CPMG), has been introduced a long time ago and used to measure ^{15}N relaxation in proteins [38–41]. Essentially all of these reports note the presence of bias in R_2 rates measured with PD-CPMG, on the order of 5% [38,39,41]. Because of this unresolved issue PD-CPMG has seen little use over the last two decades.

Here we present a new and upgraded version of PD-CPMG which can reliably reproduce the results of the well-established $R_{1\rho}$ spin-lock experiment. The new pulse sequence allows one to extend the observation window τ_{rel} to 500 ms and beyond, Fig. 1c. The proper sampling of the relaxation decay curve, down to the level of 0.2 on the relative intensity scale, facilitates the accurate determination of R_2. For the samples at hand, the precision of the relaxation measurements is improved by up to a factor of 3 compared to the standard $R_{1\rho}$ experiment. In addition to the extended observation window, the new version of PD-CPMG experiment offers a number of other valuable properties, as discussed below.

2. Results

2.1. PD-CPMG pulse sequence for ^{15}N R_2 measurements

The new pulse sequence shown in Fig. 2 is essentially a decoupled, sensitivity-enhanced HSQC, similar to what has been previously used for ^{15}N $R_{1\rho}$ measurements [10]. Inserted in this sequence is the proton-decoupled CPMG element of the net

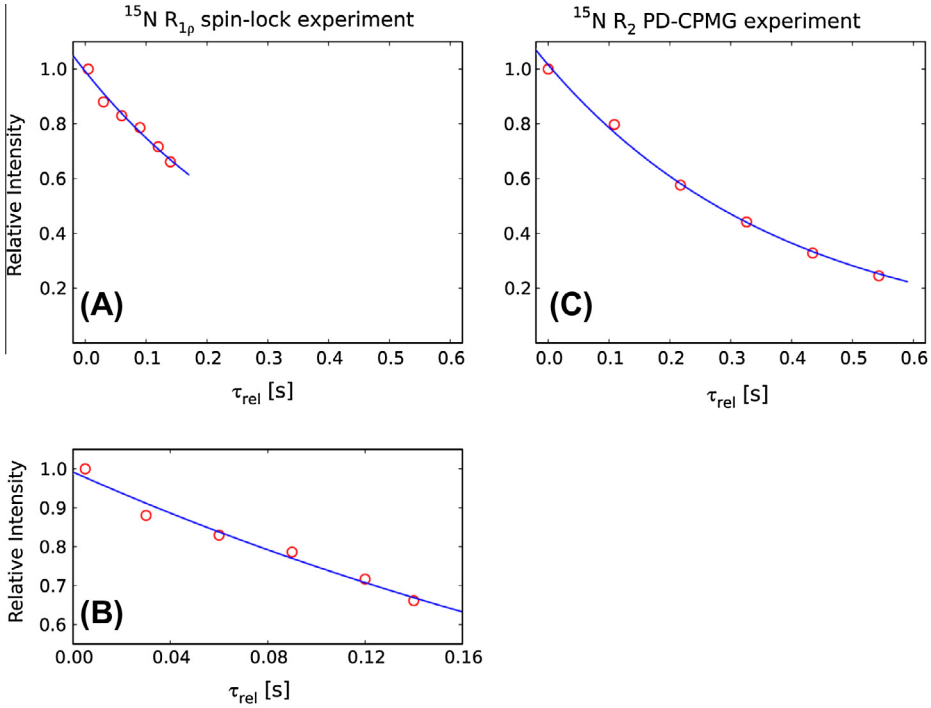

Fig. 1. Examples of relaxation curves from ^{15}N $R_{1\rho}$ spin-lock experiment (panels A and B) and R_2 PD-CPMG experiment (panel C). The data are from residue L15 in 100 μM sample of unfolded ubiquitin at 37 °C. Panel (B) is the expansion of panel (A).

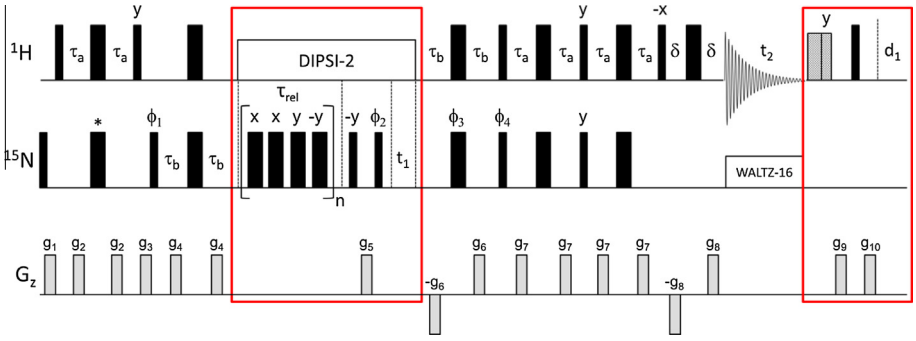

Fig. 2. PD-CPMG pulse sequence for measuring ^{15}N R_2 relaxation rates. The design is based on the experiment by Korzhnev et al. [10]; the portions of the sequence which are new and distinct are enclosed in red boxes. The pulse and delay settings listed below are for the measurements on denatured ubiquitin (see Section 5 for sample conditions). Hard ^{1}H pulses are applied with the carrier set on water resonance and *rf* field strength of 40 kHz. Two consecutive water purge pulses [51] have the durations of 6.0 and 3.7 ms and use the *rf* field of 12.4 kHz (shaded rectangles in the plot). DIPSI-2 decoupling [46] is applied with the carrier shifted to the middle of the amide region (8.3 ppm). The decoupling *rf* field corresponds to 90° pulse of duration 61 μs (*rf* field strength 4.1 kHz). Considering that one DIPSI-2 cycle corresponds to 10,360° rotation, the duration of the cycle is determined to be Δ_{DIPSI2} = 7.0218 ms. The ^{15}N CPMG sequence is applied in a form of $[\tau_{CP} - 180°_x - \tau_{CP} - \tau_{CP} - 180°_x - \tau_{CP} - \tau_{CP} - 180°_y - \tau_{CP} - \tau_{CP} - 180°_{-y} - \tau_{CP}]_n$ pulse train, where n is an integer number. When n = 0 this element becomes nil, i.e. it does not contain any pulses or delays. The interval between the consecutive 180° ^{15}N CPMG pulses should be adjusted according to the synchronization condition $2\tau_{CP} + p_{N(180)} = m\Delta_{DIPSI2}$, where $p_{N(180)}$ is the duration of 180° ^{15}N pulse and m is an integer number. In our main series of measurements we used the setting m = 2 corresponding to $2\tau_{CP}$ = 13.9676 ms. All ^{15}N pulses, including 180° CPMG pulses, have been applied with the maximum *rf* field strength, in our case 6.6 kHz ($p_{N(180)}$ = 76 μs). WALTZ-16 decoupling during the acquisition period employs 1.1 kHz *rf* field. The delay settings are τ_a = 2.25 ms, $\tau_b = 1/(4J_{NH})$ = 2.75 ms, and δ = 0.75 ms. The recycling delay employed is d_1 = 2 s. Gradient strengths in G/cm (length in ms) are g_1 = 5.0 (1.0), g_2 = 4.0 (0.5), g_3 = 10.0 (1.0), g_4 = 8.0 (0.5), g_5 = 25.0 (1.0), g_6 = 15.0 (1.25), g_7 = 4.0 (0.5), g_8 = 14.8 (0.125), g_9 = 20.0 (3.5), g_{10} = 20.0 (2.0). The phase cycle employed is ϕ_1 = (x, −x), ϕ_2 = y, ϕ_3 = 2(x), 2(y), 2(−x), 2(−y), ϕ_4 = x, ϕ_{rec} = (x, −x, −x, x), with DIPSI-2 *rf* field applied along x. Quadrature detection in F_1 is achieved by using the enhanced sensitivity approach [52,53] whereby separate spectra are recorded with (ϕ_4, g_6) and (ϕ_4 + π, $-g_6$) settings for each t_1 increment. Phase ϕ_2 is inverted in concert with the receiver phase for each t_1 increment such as to shift axial peaks to the edge of the spectrum [54]. While the sequence is primarily aimed at the backbone amide sites, it can also be adapted to measure arginine side-chain $^{15}N^{\varepsilon}$ R_2 relaxation rates. For this purpose ^{15}N carrier needs to be set to 85 ppm, rectangular ^{15}N 180° pulse marked by (*) should be replaced with r-SNOB pulse [55] with ca. 15 ppm bandwidth, and ^{15}N 180° pulses in the CPMG train need to be changed into REBURP shapes [56] with ca. 15 ppm bandwidth covering $^{15}N^{\varepsilon}$ resonances, but not $^{15}N^{\eta}$.

duration τ_{rel}. The CPMG pulse train uses [0013] phase cycle which was recently shown to have favorable compensation properties [42–45]. The pulse repetition rate in the PD-CPMG sequence is relatively low, with the pulse spacing $2\tau_{CP}$ ca. 14 ms. The proton decoupling during the CPMG train is achieved by application of the DIPSI-2 sequence [46] with the *rf* field strength 4 kHz. The relatively low level of combined ^{1}H and ^{15}N *rf* power allows us to extend τ_{rel} period to 500 ms and beyond.

In the pulse sequence Fig. 2 proton decoupling is extended to also cover t_1 evolution period. It is well known that proton decoupling during t_1 generally leads to sharper spectral peaks [47,48]. This is particularly important for IDPs where the spectra are highly crowded. Under physiological conditions, IDPs experience fast solvent exchange which efficiently destroys two-spin modes such as $2N_xH_z$ [49]. For conventional HSQC experiment, this causes substantial line broadening in ^{15}N dimension resulting in poor-quality

spectra. In contrast, decoupled HSQC experiment records the evolution of pure in-phase coherence, N_x, and therefore avoids this problem. The sequence shown in Fig. 2 is conceptually similar to the previously published scheme [50], although the objectives of the two experiments and the technical details are different (discussed later in the article).

As discussed in detail below, the ^{15}N 180° CPMG pulses should be calibrated with care for the purpose of PD-CPMG measurements. However, standard calibration scheme is sufficient – we recommend using the HSQC-based calibration experiment.[1] The calibration of proton 90° pulse for DIPSI-2 decoupling does not need to be particularly accurate since PD-CPMG sequence is highly tolerant to pulse calibration errors. It is advisable to use the HSQC-based calibration experiment, but water-based calibration is also acceptable. It is important, however, that the duration of τ_{CP} is calculated rigorously according to the synchronization condition. For example, the experiment described in Fig. 2 was set up with $2\tau_{CP}$ = 13.9676 - ms, even though for the sake of brevity we refer to it as $2\tau_{CP}$ = 14 ms (see figure caption for details).

Note that fast solvent exchange partially cancels the advantage of the sensitivity enhancement in the pulse sequence Fig. 2. A maximum potential gain from the use of the sensitivity enhancement scheme is given by a factor $\sqrt{2}$. However, the sequence requires an extra transfer step of ca. 5 ms duration. Assuming that amide solvent exchange rate is 100 s^{-1}, it is easy to estimate that the loss of signal due to solvent exchange completely offsets the sensitivity gain. Nevertheless, for most samples of practical interest the exchange rate is lower than 100 s^{-1} and therefore the use of the sensitivity enhancement scheme is likely justified (also due to its excellent water suppression properties).

Finally, under the conditions of fast solvent exchange there is a potential risk associated with partial saturation of the water signal [57,58]. Generally speaking, the degree of saturation is variable and, in particular, depends on τ_{rel}. Since the saturation is effectively transmitted to the amide sites, the magnitude of $^1H^N$ magnetization available prior to each scan also turns out to be dependent on τ_{rel}. This causes an unwanted modulation of the measured relaxation curves, which can seriously compromise the accuracy of the experiment [59,60]. To avoid these artefacts we have chosen to "crush" water magnetization following the acquisition period and prior to the recycling delay, thus creating highly reproducible initial conditions. This design leads to a very accurate experiment. In principle, the sensitivity is to a certain degree sacrificed relative to a sequence that preserves water magnetization. However, in practice the sensitivity is similar to the standard ^{15}N relaxation experiments where the water signal is strongly saturated with no regard for solvent exchange.

2.2. The results from PD-CPMG are consistent with ^{15}N spin-lock experiment

In order to confirm that PD-CPMG scheme achieves consistency with other commonly used R_2 measurement strategies such as ^{15}N spin-lock experiment, we have collected both types of data on the samples of chicken α-spectrin SH3 domain (1.5 mM) and unfolded ubiquitin (2.0 mM). Only those peaks that do not have any significant spectral overlaps have been selected for processing and analyses (58 residues for α-spc SH3 domain and 48 residues for unfolded ubiquitin). The quality of the relaxation curves is excellent in both experiments, with very low fitting residual. Importantly, the results of the two independent measurements show an excellent correlation with each other, as evidenced by the correlation coefficients 0.999 and 0.993, see Fig. 3. The systematic deviation between the two datasets is very small. Specifically, the difference between the mean values of R_2 from the new PD-CPMG experiment and the standard spin-lock experiment is +0.9% in the case of α-spc SH3 and −1.3% in the case of ubiquitin. Even though such differences are negligibly small, we have a fairly good idea of what causes them. In the case of ubiquitin, the conductivity of the acidic sample is relatively high and therefore it experiences a substantial amount of heating [61]. PD-CPMG sequence heats the sample a little more than spin-lock sequence, 0.45 vs. 0.30 °C, leading to slightly lower R_2 rates. For α-spc SH3 the amount of heating generated by both experiments is small, less than 0.1 °C. However, one has to bear in mind that α-spc SH3 is a folded protein with broadly dispersed $^1H^N$ spectrum. DIPSI-2 decoupling does not work quite as well in this case, leading to a small magnetization loss and consequently slightly overestimated R_2 rates. Both aspects – the performance of proton composite decoupling and sample heating – are discussed in greater detail in what follows.

We have also recorded a control PD-CPMG experiment where the strength of the DIPSI-2 decoupling was lowered from ca. 4 kHz to ca. 3 kHz. The results remain virtually unchanged, as illustrated in Fig. 4 (correlation coefficients 0.999 and 0.998). The observed amount of systematic deviation is vanishingly small (and can be rationalized along the same lines as above). Importantly, this result means that PD-CPMG experiment with relatively low level of decoupling power, ca. 3 kHz, can be used to sample the relaxation profiles up to $\tau_{rel} \sim 1$ s and beyond. It can also be used to collect the data from samples with high conductivity (high ionic strength) where sample heating due to deposition of the *rf* power needs to be reduced.

2.3. PD-CPMG scheme improves the precision of ^{15}N R_2 measurements

The PD-CPMG sequence is intended to improve the sampling of ^{15}N relaxation curves in the situation when R_2 relaxation is relatively slow, on the order of 1–3 s^{-1}. Specifically, the experiment is relevant for IDPs at or near the physiological temperature. Of necessity, NMR studies of IDPs are often conducted at low concentration, 100 μM or less. Furthermore, the time frame of the measurements is usually limited, since the samples have a tendency to rapidly deteriorate. For those samples where pH is close to physiological, the signal-to-noise ratio is further lowered by amide solvent exchange which in the case of IDPs affects all residues in the protein. Under these circumstances, the precision of ^{15}N R_2 data can become a critical issue.

In order to model this type of a situation, we have prepared two samples of unfolded ubiquitin with protein concentration 100 and 50 μM and collected the relaxation data at 37 °C. Toward this end, we employed the standard ^{15}N $R_{1\rho}$ experiment [10] as well as the new PD-CPMG scheme. All experiments were recorded in duplicate to assess the reproducibility of the results. The outcome is illustrated in Figs. 5 and 6.

The relaxation curves recorded in the repeat spin-lock and PD-CPMG experiments are illustrated in Fig. 5. The results for residue L15 are shown as is, i.e. in a form of $R_{1\rho}$ decay and apparent R_2^{app} decay, with no correction for ^{15}N frequency offset. The quality of the fits is similar for the two experiments, as can be appreciated from the magnitude of the fitting residual χ. However, the reproducibility of the relaxation rates as determined in the spin-lock measurements (2.41 and 2.81 s^{-1}) is clearly worse than for PD-CPMG (2.67 and 2.56 s^{-1}). This happens because the spin-lock experiment is limited to short τ_{rel} delays and therefore cannot properly sample the relaxation decay profile [34].

The summary of the data from the repeat experiments is shown in Fig. 6. Clearly, PD-CPMG achieves a much better reproducibility

[1] Specifically, 1D version of $^1H^N$–^{15}N HSQC, where a variable-length nitrogen pulse is inserted following the initial INEPT period (Daiwen Yang and Lewis Kay, unpublished).

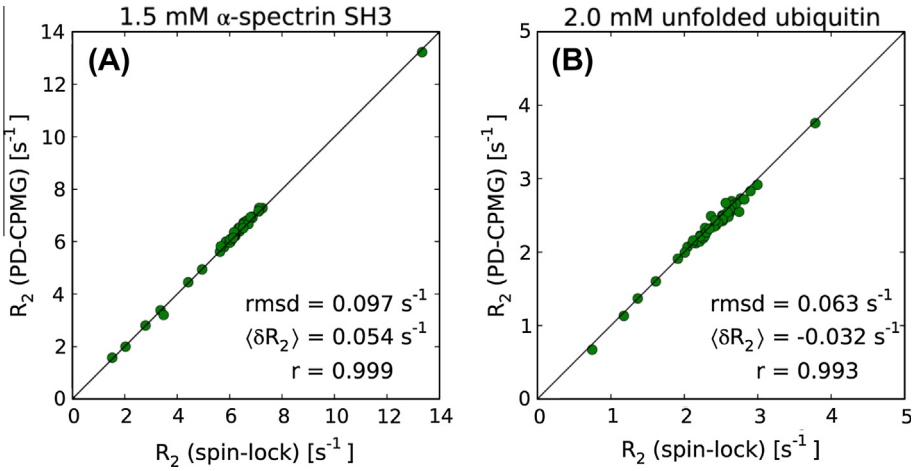

Fig. 3. Comparison of ^{15}N R_2 rates from the PD-CPMG experiment and the standard spin-lock measurement [10]. Each experiment took ca. 2 h to record. The PD-CPMG experiment used 4 kHz DIPSI-2 decoupling. All datasets have been corrected for ^{15}N frequency offset effects (see below for details). PD-CPMG experiment on the sample of α-spc SH3 was carried out with $2\tau_{CP}$ = 13.7373 ms and the set of six τ_{rel} delays ranging from 0 to 275 ms.

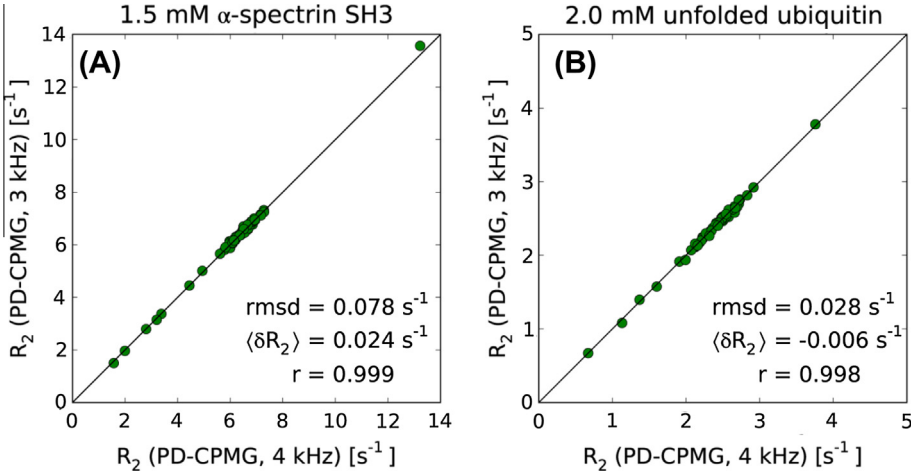

Fig. 4. Comparison of ^{15}N R_2 rates from the PD-CPMG measurements using ca. 4 kHz and 3 kHz DIPSI-2 decoupling. In the experiments with 3 kHz decoupling, the data from α-spc SH3 were obtained using m = 1, $2\tau_{CP}$ = 9.6509 ms, and the set of six τ_{rel} delays ranging from 0 to 193 ms, whereas the data from ubiquitin were collected using m = 1, $2\tau_{CP}$ = 9.8235 ms and the set of six τ_{rel} delays ranging from 0 to 589 ms.

than the standard spin-lock measurement [10]. The average absolute-value error in $R_{1\rho}$ data is three times as large as in PD-CPMG R_2^{app} data: 9.1% vs. 3.7% for 100 μM sample and 22.6% vs. 7.5% for 50 μM sample. This difference in precision can be critical for studies that use ^{15}N relaxation to quantify changes in IDPs conformational dynamics in response to various perturbations, e.g. point mutations, posttranslational modifications, variations in pH, crowding effects, etc. Such changes are typically subtle and can be successfully identified only when high-precision ^{15}N relaxation data are available. Note that $R_{1\rho}$ data shown in Fig. 6c are essentially useless in this regard since the measurement errors are of the same magnitude as per-residue R_2 variations. In contrast, R_2^{app} data shown in Fig. 6d retain the ability to distinguish between mobile residues, constrained residues, and those residues that experience exchange broadening.

2.4. Modified PD-CPMG scheme for arginine side-chain $^{15}N^{\varepsilon}$

After small modifications, the PD-CPMG scheme Fig. 2 can also be used to measure R_2 relaxation rates of $^{15}N^{\varepsilon}$ spins in Arg side chains. Arginine side chains are long and flexible; in globular proteins they are typically immersed in solvent and move in a relatively unconstrained fashion. Consequently, $^{15}N^{\varepsilon}$ R_2 rates tend to be low compared to the backbone ^{15}N rates and thus particularly well suited for PD-CPMG measurements. It is also worth noting that N^{ε} are more prone to solvent exchange than the backbone amide sites. Therefore, the favorable properties of the PD-CPMG experiment with regard to solvent exchange are especially useful in the context of $^{15}N^{\varepsilon}$ measurements.

The pulse sequence requires some alterations, as described in the caption of Fig. 2. The main source of difficulties is the weak $^{15}N^{\varepsilon}$–$^{15}N^{\eta}$ two-bond coupling with the magnitude ca. 1 Hz [62]. This coupling remains active during the standard CPMG pulse train which employs hard nitrogen pulses. Since τ_{rel} times employed in our measurements are long, the $^2J_{N\varepsilon N\eta}$ coupling achieves partial conversion of N_x^{ε} into $2N_y^{\varepsilon}N_z^{\eta}$ during this time period. This causes partial loss of signal and distorts the observed relaxation decay profiles.

Since $^{15}N^{\varepsilon}$ and $^{15}N^{\eta}$ have significantly different chemical shifts (separated in the spectrum by ca. 10 ppm), this problem can be easily overcome by application of selective 180° pulses during the CPMG period. For this purpose we have employed REBURP

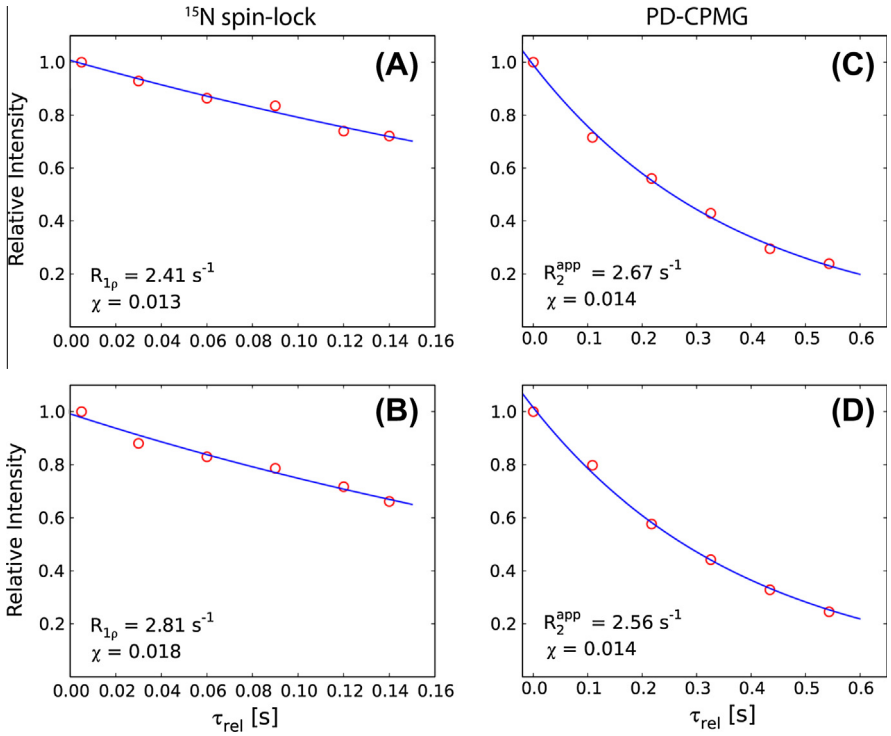

Fig. 5. Relaxation decay profiles for residue L15 in 0.1 mM sample of unfolded ubiquitin as obtained from the repeat measurements using ^{15}N spin-lock experiment (panels A and B) and PD-CPMG (panels C and D). For reference, the measurements using 2.0 mM sample of unfolded ubiquitin yield $R_{1\rho} = R_2^{app} = 2.58$ s^{-1} (uncorrected for ^{15}N offset effects). Parameter χ indicated in the plot is the rmsd between the experimental and fitted intensities.

pulses which have been used in the context of CPMG measurements before [63,64]. One of the potential problems with such strategy is that REBURP pulses are relatively long, 4.0 ms, so that nitrogen magnetization spends part of the time away from the transverse plane. As a result, the measured relaxation decay may potentially represent a mixture of R_2 and R_1 rates. However, numerical simulations suggest that this effect introduces only a very small error, on the order of 1%. To understand this result, one should take into consideration several factors. (i) REBURP pulses are applied relatively infrequently, $2\tau_{CP} \geqslant 10$ ms. (ii) REBURP pulses are applied on-resonance or close to resonance (since $^{15}N^{\varepsilon}$ chemical shifts are confined to a relatively narrow range). Under these conditions the magnetization mostly remains in the transverse plane during the REBURP pulse. (iii) REBURP pulses are applied with [0013] phase cycle. Considering N_x magnetization, we observe that it is locked by the first two pulses, such that no R_1 character is introduced into spin relaxation. Similarly N_y magnetization is locked by the last two pulses. (iv) In rapidly moving Arg side chains, R_2 and R_1 rates tend to be similar.

Ultimately we rely on the comparison with $R_{1\rho}$ experiment to confirm that PD-CPMG measurement is error-free. Importantly, $R_{1\rho}$ experiment is insensitive to the effect of $^2J_{N\varepsilon N\eta}$. Numerical simulations show that given a relatively large chemical shift offset between $^{15}N^{\varepsilon}$ and $^{15}N^{\eta}$, ca. 10 ppm, moderate spin-lock strength, ~1.5–2 kHz, very weak coupling, ~1 Hz, and relatively short τ_{rel} delays, ~100 ms, it is safe to neglect Hartmann–Hahn transfer during the spin-lock period. In Fig. 7 we compare the R_2 rates obtained from the standard $R_{1\rho}$ experiment with those measured by $^{15}N^{\varepsilon}$ PD-CPMG. The two datasets are consistent within 0.5%, which is approximately the same as the level of agreement previously observed for the backbone amide sites, see Fig. 3a. This result provides validation for the modified version of the PD-CPMG sequence aimed at $^{15}N^{\varepsilon}$ spins. Potential gains in precision in this case should be even more significant than for backbone measurements.

3. Experimental details

3.1. ^{15}N offset dependence

One significant shortcoming of the traditional CPMG experiment is that it requires a numerical procedure to correct for ^{15}N offset effect [65]. In contrast, the PD-CPMG experiment using [0013] phase cycle allows for a simple analytical correction [44]:

$$R_2^{app} \approx R_2 + (R_1 - R_2)\mu^2 \quad (1)$$

$$\mu = \nu_{off}^{N}/\nu_1^{N(180)}$$

Here R_2^{app} is the apparent decay rate as derived directly from the PD-CPMG measurement, ν_{off}^{N} is the nitrogen frequency offset for a given amide resonance, and $\nu_1^{N(180)}$ is the field strength of the hard ^{15}N 180° CPMG pulses in the units of Hz. For the experimental settings used in this study the magnitude of μ^2 does not exceed 0.03. Consequently, it is safe to ignore higher-order corrections which are proportional to μ^4.

The formula Eq. (1) reflects the fact that during τ_{rel} period (or more specifically during $2\tau_{CP}$ intervals) ^{15}N magnetization moves on a path which takes it away from the transverse plane. By the end of each [0013] cycle, however, the magnetization is returned to the transverse plane as a result of the good self-compensation properties of this cycle. The original correction formula published by Bain et al. contains an extra term which describes spin relaxation during ^{15}N 180° pulses [44]. In our case this additional term can be safely neglected because ^{15}N 180° pulses are very short compared to $2\tau_{CP} \geqslant 10$ ms. The resulting simple expression Eq. (1) can be easily inverted to determine the true relaxation rate constant R_2.

The validity of Eq. (1) has been tested by means of numeric simulations. Briefly, spin evolution in the two-spin ($^1H^N$, ^{15}N) system was modeled using full product operator basis of dimension 15.

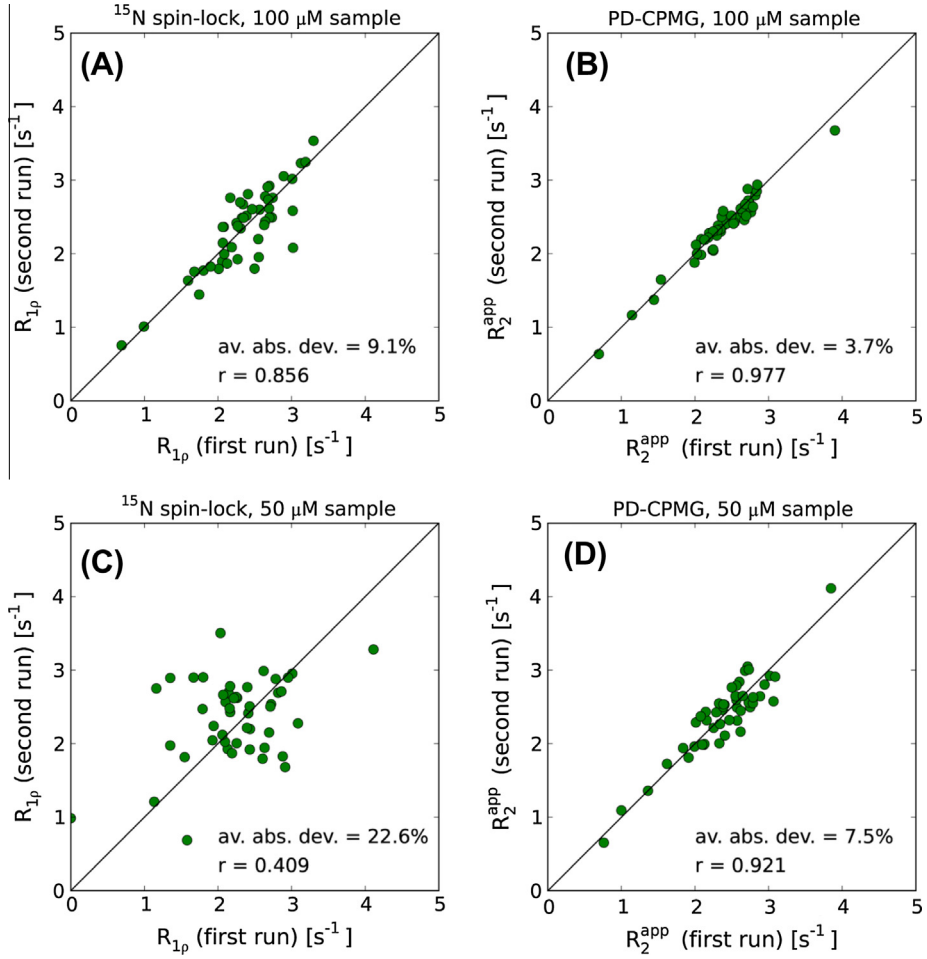

Fig. 6. The reproducibility of $R_{1\rho}$ and R_2^{app} relaxation rates as measured in the repeat spin-lock and PD-CPMG experiments using low-concentration samples of unfolded ubiquitin at 37 °C. Each experiment was recorded in a total of ca. 2 h.

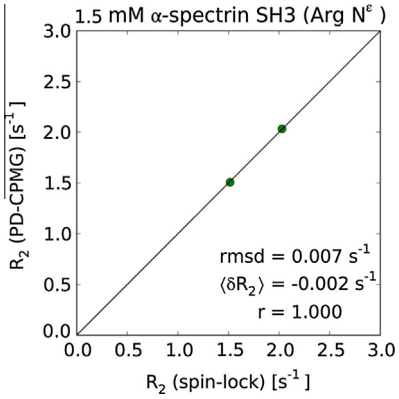

Fig. 7. Comparison of arginine $^{15}N^{\varepsilon}$ R_2 rates from the PD-CPMG experiment and the standard spin-lock measurement. The results are from two arginine residues in α-spc SH3 domain, R21 and R49. Protein concentration in the sample is 1.5 mM. The PD-CPMG sequence has been adapted to measure $^{15}N^{\varepsilon}$ relaxation as discussed in the text. In running this experiment one has to be mindful of $^{15}N^{\varepsilon}$ and $^{15}N^{\eta}$ chemical shifts specific to a given protein. The spin-lock sequence [10] was used as is, with nitrogen *rf* carrier set to 85 ppm. Both datasets have been corrected for ^{15}N frequency offset effects.

All coherent evolution mechanisms were included (chemical shift, *rf* pulses, scalar coupling) as well as the standard relaxation mechanisms (dipolar and CSA). In terms of *rf* pulses, the simulations reproduce the experimental setup described in the caption of Fig. 2. We have also included the effects of ^{15}N *rf* field inhomogeneity which was modeled via Gaussian distribution with the width $2\sigma = 0.1 \times \nu_1^N$. Further details can be found in Materials & Methods.

In Fig. 8a we illustrate the dependence of the apparent R_2^{app} rate on ^{15}N frequency offset ν_{off}^N. Shown are the simulated R_2^{app} rates (red circles) as well as the predictions using Eq. (1) (black curve). The true value of R_2 is indicated by the horizontal dashed line. This result suggests that the rates measured via PD-CPMG experiment and corrected by means of Eq. (1) provide a very accurate measure of R_2 relaxation.

Note also that the offset dependence illustrated in Fig. 8a is rather weak. This is not surprising since PD-CPMG employs a train of hard ^{15}N 180° pulses which effectively refocus nitrogen magnetization across the entire spectrum. In fact, if the offset dependence is ignored the resulting error in determination of R_2 does not exceed 1%. In most cases the error of this magnitude can be tolerated and therefore it is safe to assume that $R_2 = R_2^{app}$. This obviates the need in ^{15}N R_1 measurement which is otherwise needed to calculate the offset correction according to Eq. (1). Finally, it is worth noting that the result shown in Fig. 8a is independent of the *rf* field

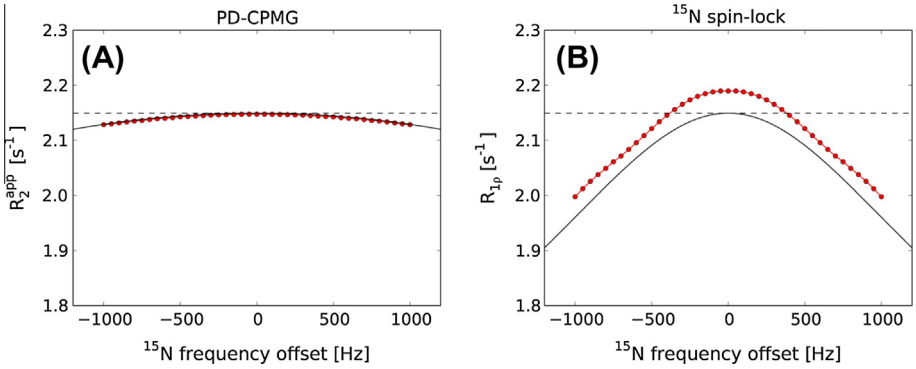

Fig. 8. Simulated dependencies (A) R_2^{app} vs. ν_{off}^N for the PD-CPMG experiment and (B) $R_{1\rho}$ vs. ν_{off}^N for the spin-lock experiment. The results from numeric simulations are shown with red circles (red lines), the calculations using analytical formulas are shown with solid black lines, the target value of R_2 is shown with the horizontal dashed line. The CPMG and spin-lock pulse sequence elements are modeled with the same settings as used in the experimental study (see Fig. 2 and Section 5). In particular, proton DIPSI-2 decoupling is assumed to be applied on-resonance with the *rf* field strength 4 kHz.

inhomogeneity on both ^{15}N and ^{1}H channels (assuming any reasonable *rf* field distribution).

For comparison, in Fig. 8b we show the equivalent dependence for the spin-lock experiment, $R_{1\rho}$ vs. ν_{off}^N [10]. Notably, there is a shift between the simulated $R_{1\rho}$ rates (red circles) and the standard correction formula, $R_{1\rho} = R_2 \sin^2\theta + R_1 \cos^2\theta$ (black curve). The shift, which has a magnitude of 0.03–0.04 s^{-1}, can also be found in the Korzhnev's original report (see Figs. 2 and 3 therein). It arises from the interplay between the spin-lock, $^1J_{NH}$ coupling, and ^{1}H 180° pulses used to suppress dipolar-CSA cross-correlations [10]. Even though such pulses are applied infrequently, they can still give rise to a discernible error. In relative terms, this error can be safely neglected for slowly tumbling globular proteins, but not necessarily so for highly mobile IDPs.

As it turns out, in the case of high-conductivity ubiquitin sample the systematic error associated with spin-lock experiment, Fig. 8b, is compensated by the effect from sample heating (see below). Such error cancelation, however, is fortuitous. For samples with low conductivity the error would persist at the level of ca. 2%. Furthermore, the magnitude of the error is sensitive to the details of ^{15}N *rf* field inhomogeneity and may potentially increase beyond this level.

3.2. ^{1}H decoupling and choice of τ_{CP}

As already pointed out, proton decoupling should be synchronized with ^{15}N CPMG pulse train according to

$$2\tau_{CP} + p_{N(180)} = m\Delta_{DIPSI2} \quad (2)$$

For this purpose, one should calibrate the proton 90° pulse at the chosen decoupling power (3–4 kHz), calculate the duration of the decoupling cycle Δ_{DIPSI2}, and then set τ_{CP} accordingly (see caption of Fig. 2).

What happens if the synchronization condition is not met? DIPSI-2 sequence is designed to achieve near-complete suppression of $^1J_{NH}$ over the time period Δ_{DIPSI2}. However, if at some point during Δ_{DIPSI2} one applies a ^{15}N 180° pulse this would interfere with the decoupling scheme, leading to less-than-perfect suppression of $^1J_{NH}$. As a consequence, nitrogen spin would experience a certain amount of scalar-coupled evolution and suffer from additional magnetization loss (e.g. due to dephasing of $2N_yH_z$ under the effect of the proton *rf* field). From the perspective of PD-CPMG measurements, this would result in overestimated nitrogen R_2 rates. Indeed, we have been able to reproduce this effect via simulations and experimentally. When PD-CPMG experiment is set up with no regard for synchronization conditions, the determined R_2 rates prove to be systematically higher. For example, in trial experiments involving unfolded ubiquitin we observed the bias of ca. 0.07 s^{-1}. While such relatively small deviations can usually be neglected for slowly tumbling globular proteins, they are not necessarily insignificant in the case of IDPs.

The undesirable effects can be avoided by enforcing the synchronization condition Eq. (2). In principle, the value of m used in the synchronization condition should be even. However in practice odd values of m are equally acceptable (verified both experimentally and by simulations). This is so because one-half of the standard DIPSI-2 cycle still offers excellent decoupling properties. For example, in the case of ubiquitin measurements described in the caption of Fig. 2 the synchronization condition reads $2\tau_{CP}$ = (-m·7.0218–0.0760) ms, where m = 1, 2, 3, ...

The choice m = 2 corresponds to the strength of the effective *rf* field $\nu_1^{CPMG} = 1/4\tau_{CP} = 36$ Hz. This is much lower than the strength of the *rf* field used for proton decoupling, 4.1 kHz. Thus, the experiment should be safe with regard to a potential risk of Hartmann–Hahn transfer. Indeed, our simulations predict that the outcome of the experiment is independent of the choice of m, confirming that Hartmann–Hahn transfer is not an issue.

However, the experimental tests revealed a different type of complication. As it turns out, the measurements using large values of m (i.e. long τ_{CP} delays) yield slightly higher than expected R_2 rates. For instance, in the case of ubiquitin, increasing m from 2 to 6 leads to 0.1 s^{-1} increase in the average R_2 value. The trend is reverse of what could be expected from Hartmann–Hahn cross-polarization. It also cannot be explained by a variable degree of sample heating (the effect is also observed in α-spectrin SH3, where there is very little heating). We have considered a number of possible scenarios: (i) dispersion-like effect associated with pervasive small R_{ex} contributions; (ii) the effect from small scalar couplings between ^{15}N and $^1H^\alpha$, $^1H^\beta$; (iii) the effect from small scalar couplings between ^{15}N and natural-abundance ^{13}C; (iv) the effect of dipole–dipolar cross-correlations in a three-spin system ^{15}N, $^1H^N$, and $^1H^\alpha$ ($^1H^\beta$); (v) the effect of diffusion (convection flow) in inhomogeneous static magnetic field. Using additional experimental tests and/or numeric simulations we were able to rule out each of these explanations.

Instead, we hypothesize that the performance of DIPSI-2 decoupling is not quite as efficient as suggested by numeric simulations. Small instrumental defects such as finite pulse rise time, phase transients, or amplifier drooping have a subtle, yet discernible effect on the real-life performance of the decoupling sequence. To demonstrate the feasibility of this hypothesis we conducted additional experimental measurements. Specifically, the PD-CPMG experiment was repeated with ^{1}H *rf* carrier shifted from 8.3 ppm to 6.5 ppm. The numeric simulations (including carefully designed

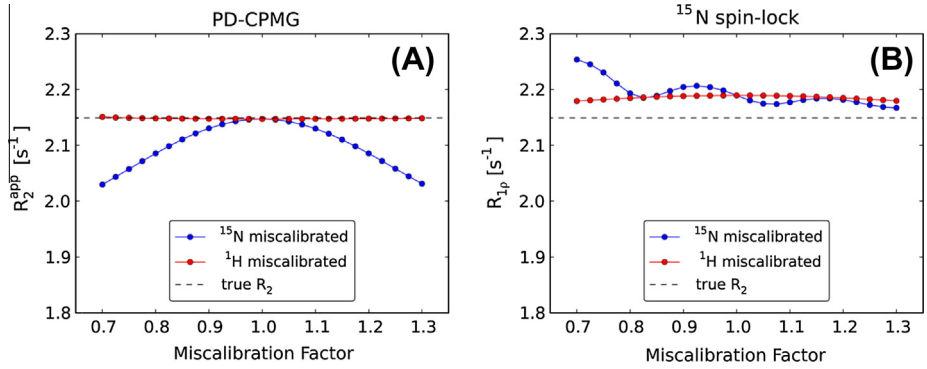

Fig. 9. The effect of *rf* pulse miscalibration on (A) R_2^{app} rates from PD-CPMG experiment and (B) $R_{1\rho}$ rates from spin-lock experiment. The miscalibration factor represents the ratio of the actual ν_1 to the target ν_1. The simulations have been conducted assuming $\nu_{off}^N = 0$ and $2\sigma = 0.1 \times \nu_1^N$. For proton channel, the effects of frequency offset and *rf* field inhomogeneity were found to be negligibly small.

three-spin simulations) predict that such carrier jump should have no effect on the measured R_2 rates. Yet the experimentally measured R_2 values in the sample of unfolded ubiquitin increased on average by 0.03 s^{-1}. In the case of α-spc SH3 with its widely dispersed $^1H^N$ spectrum the increase was more substantial, 0.06 s^{-1}. This lends support to our hypothesis that the real-life performance of proton decoupling is less perfect than can be inferred from the simulations.

This result makes us suggest that DIPSI-2 decoupling is less efficient than expected in suppressing $^1J_{NH}$ coupling. In this situation we rely on ^{15}N 180° pulses to assist with decoupling. In order to fully suppress $^1J_{NH}$ evolution, nitrogen pulses should be applied sufficiently frequently. It is also important that nitrogen pulses are applied with maximum power, in our case 6.6 kHz.[2] To summarize, the PD-CPMG experiment presented in this paper should be executed with proton decoupling *rf* power of 3–4 kHz and $2\tau_{CP}$ ~ 10–15 ms (subject to synchronization condition, m = 1–2). Use of the lower decoupling power or longer τ_{CP} delays results in a small but measurable bias, leading to overestimated R_2 rates.

Finally, we would like to comment on the choice of proton decoupling scheme. DIPSI-2 was selected primarily for its excellent J-coupling suppression properties. The decoupling bandwidth is a secondary consideration (particularly for disordered proteins with their narrow range of $^1H^N$ chemical shifts). The PD-CPMG measurements using DIPSI-3 decoupling produce the results that are virtually identical to those obtained with DIPSI-2. Choosing between the two, we prefer the latter scheme since it offers a benefit of a shorter cycle. Accurate results have also been obtained using WALTZ-16. However, in this case the experiment becomes more sensitive to synchronization condition – away from the correct setting expressed by Eq. (2) the measured R_2 rates turn out to be significantly overestimated (confirmed both experimentally and by simulations). Along these lines we can explain the appearance of bias in the earlier implementations of PD-CPMG [38]. Finally, GARP-1 decoupling sequence shows relatively poor performance. This is not surprising since GARP offers excellent bandwidth, but mediocre J-coupling suppression properties [66].

3.3. Rf pulse miscalibration

The numeric simulations modeling the effect of *rf* pulse miscalibration on the measured R_2^{app} and $R_{1\rho}$ rates are illustrated in Fig. 9. The PD-CPMG experiment turns out to be remarkably stable with respect to miscalibration of proton pulses in the DIPSI-2 decoupling scheme (red circles[3] in Fig. 9a). This reflects excellent self-compensation properties of the DIPSI-2 sequence as manifested in our simulations. On the other hand, the miscalibration of ^{15}N 180° pulses leads to nitrogen magnetization spending part of the time away from the transverse plane. This results in the increased R_1 character of the spin relaxation and lower R_2^{app} rates (blue circles). Note that in practice ^{15}N pulse calibration should be accurate to at least within ±5%. Hence the actual miscalibration factor is likely confined to the narrow range 0.95–1.05. In this range the R_2^{app} rates obtained from the PD-CPMG measurements remain essentially unchanged. We have also considered the scenario where both ^{15}N and ^{1}H pulses are miscalibrated. The results are no different from the situation where ^{15}N pulses alone are misset.

As a point of comparison, the effect of *rf* field miscalibration on $R_{1\rho}$ experiment is also illustrated, Fig. 9b. There is certain amount of error associated with this experiment as manifested in the shift between the simulated and the target relaxation rates (see Fig. 8 and related discussion). Varying the strength of on-resonance ^{15}N spin lock in the interval from 1.2 to 2.2 kHz modulates the magnitude of error as shown in the plot; the sinusoidal modulation pattern is similar to the one previously observed [10]. There is also an additional element of bias associated with spin-lock experiment which is not reflected in Fig. 9b. The failure to correctly determine ν_1^N leads to an error in applying the ^{15}N offset correction. The amount of error can be substantial, on the order of 0.1 s^{-1}. This is much worse than in the case of PD-CPMG experiment, which is fairly insensitive to the ^{15}N offset effects (see Fig. 8).[4]

Finally, we have conducted additional experimental measurements to test the validity of the simulations illustrated in Fig. 9a. For this purpose we have deliberately misset the proton pulse in the DIPSI-2 decoupling sequence – instead of the properly calibrated value, $p_{H(90)}$ = 61 μs, we have used 56 or 66 μs. Using this altered experimental setup, we repeated the PD-CPMG measurements on the sample of unfolded ubiquitin. The results proved to be in perfect agreement with the previously obtained data, thus confirming that PD-CPMG experiment is immune to miscalibration of the DIPSI-2 proton pulses. Along the same lines we have tested the incorrect settings for nitrogen CPMG pulses: instead of $p_{N(180)}$ = 76 μs we have used 66 or 86 μs. As expected, this led to appreciable decreases in the measured R_2 rates (on average by 0.09 and 0.06 s^{-1}, respectively). One should keep in mind, however, that these tests involve a significant element of exaggeration. In

[2] If CPMG pulses are applied with reduced level of power (4 kHz) some of the recorded decay curves become slightly distorted. This effect occurs only at certain specific values of ^{15}N frequency offset.

[3] For interpretation of color in Fig. 9, the reader is referred to the web version of this article.

[4] As for the proton pulses, their sole purpose in the spin-lock experiment is to suppress the dipolar-CSA cross-correlation. In this role they remain efficient even when their actual flip angle is varied between 130° and 230° (red circles in Fig. 9b).

practice, hard ^{15}N pulses are calibrated with much better accuracy, on the order of ±1 μs. Under these conditions the PD-CPMG experiment is essentially insensitive to the effects of pulse miscalibration.

3.4. The importance of using external ^2H lock

It is clearly desirable to study IDPs at or near physiological conditions. However, so far such studies have been rare [67]. The main difficulties arise from fast solvent exchange, $k_{ex} \sim 10–100\ s^{-1}$, which undercuts the sensitivity of HSQC experiment and worsens the situation with spectral overlaps. There are also other, more technical, problems associated with solvent exchange that can compromise the accuracy of ^{15}N relaxation measurements.

Most biological NMR samples are prepared with 5–10% D_2O for the purpose of frequency locking. However, under fast solvent exchange conditions the presence of D_2O in the sample could have a number of undesirable consequences for ^{15}N R_2 measurements [12]. (i) Standard relaxation experiments use $^1H^N(^{15}N)$ sites as a point of origin. During the course of the sequence, and in particular during τ_{rel}, the original $^1H^N(^{15}N)$ groups are partially converted into unobservable $^2H^N(^{15}N)$. This transition process modulates the recorded decay profile and thus interferes with R_2 determination. (ii) If solvent exchange is fast on the time scale of τ_{rel}, the measured R_2 rate represents a weighted average of $^{15}N(^1H^N)$ and $^{15}N(^2H^N)$ relaxation rates. (iii) In the latter case, $^{15}N(^2H^N)$ relaxation contains a sizable contribution from the scalar mechanism due to fast deuterium relaxation and solvent exchange. In PD-CPMG experiment this contribution is only partially suppressed by infrequent application of 180° ^{15}N pulses. (iv) In addition, the apparent R_2 may include an R_{ex}-type term which stems from the isotopic frequency shift between $^{15}N(^1H^N)$ and $^{15}N(^2H^N)$.

To avoid all of these complications, we use the external frequency lock, i.e. 100 μL D_2O placed in a coaxial insert fitted into the standard NMR tube. Such inserts can be purchased inexpensively from a number of vendors (we used WGS-5BL from Wilmad). They have been widely used in the past in the studies dealing with fast solvent exchange [68,69]. It has been shown that the samples using coaxial inserts are less likely to suffer from convection flow effects [70]. On the downside, such inserts are currently unavailable for Shigemi tubes.

3.5. Manipulating water magnetization

As discussed above, PD-CPMG sequence is intended for use with intrinsically disordered proteins at physiological temperature. If sample pH is also close to physiological, then solvent exchange becomes a major factor. Specifically the accuracy of the measurements can be compromised by the transfer of the saturation from water to amides mediated by fast exchange. Other transfer mechanisms, such as (i) intermolecular NOE and (ii) solvent exchange involving hydroxyl and amine groups followed by intramolecular NOE, can potentially add to the problem. Additional damage can be caused by radiation damping.

There are several ways of dealing with this complication. For instance, one can try to preserve water magnetization during the course of the pulse sequence. In principle, this is feasible since DIPSI-2 sequence can be used to lock water magnetization [71]. However, in practice this method is not well suited for our experiment. During the long τ_{rel} delays, ~ 0.5–1 s, spin-locked water magnetization undergoes significant relaxation decay and therefore fails to be conserved. The alternative approach is to use very long recycling delays allowing for complete recovery of water magnetization. For obvious reasons this is also impractical.

Instead, we have chosen to apply water purge element [51] following the acquisition period and prior to the recycling delay. This method guarantees that the amount of water magnetization present at the beginning of each scan always remains the same. Consider the situation where solvent exchange is fast on the time scale of spin–lattice relaxation, $k_{ex} \sim 10\ s^{-1}$ or higher. In this case the recovery of amide magnetization is controlled by the water R_1 rate, which is $0.2\ s^{-1}$ at 37 °C [72]. Under these circumstances, the optimal recycling delay is approximately 5.0 s. Long recovery time means that the sensitivity of the experiment suffers – it is ca. 2-fold lower compared to the schemes that preserve water magnetization. However, this is the sacrifice that is necessary to ensure the accuracy of R_2 measurements. Note that there is also a positive aspect to longer recycling delays as they help to reduce sample heating (discussed below).

The same problems are encountered in the standard relaxation experiments when applied to IDPs at or near physiological conditions. For example, in the standard $R_{1\rho}$ experiment the status of water magnetization changes depending on the number of ^1H 180° pulses applied during τ_{rel}. This gives rise to a distinctive modulation pattern in the recorded relaxation curves (data not shown). To avoid such spurious effects, we have also inserted the water-crusher element in the standard $R_{1\rho}$ pulse sequence [10]. All $R_{1\rho}$ measurements reported in this work were conducted using this amended version of the original sequence (see Materials & Methods).

3.6. Contribution from solvent exchange to R_2^{app}

Above we have discussed two potential complications associated with solvent exchange: (i) proton-deuterium exchange in a D_2O-containing sample and (ii) saturation transfer from H_2O to amide protons. In this section we discuss a third mechanism whereupon solvent exchange can interfere with ^{15}N R_2 measurements. In the absence of proton decoupling, the in-phase N_x magnetization interconverts with the anti-phase $2N_yH_z$. The latter is destroyed by solvent exchange, which physically separates the two correlated spins [49]. When solvent exchange is sufficiently fast on the time scale of $^1J_{HN}$ the resulting loss of magnetization can be described as scalar relaxation of the second kind.

In the PD-CPMG and spin-lock experiments, $^1J_{HN}$ evolution during τ_{rel} is suppressed. Therefore, one may expect that scalar relaxation should be absent. This is not quite so. For spin-lock experiment, the standard expression for scalar relaxation rate $R_2^{sc} = (\pi J_{HN})^2 \tau_{ex}/(1 + (2\pi\nu_1\tau_{ex})^2)$ [73] immediately suggests that the effect can be significant.[5] A similar outcome can be expected for the PD-CPMG experiment, although no analytical formula is available to address the situation involving DIPSI-2 decoupling.

The simulated $R_{1\rho}$ and R_2^{app} constants for a range of solvent exchange rates k_{ex} are shown in Fig. 10. The graph demonstrates that slow exchange, $k_{ex} < 10\ s^{-1}$, has virtually no effect on the extracted relaxation rates. As the exchange rate increases to $10–100\ s^{-1}$, a significant amount of error is generated. The $R_{1\rho}$ experiment using 1 kHz spin lock is particularly vulnerable (green curve). The $R_{1\rho}$ experiment using 2 kHz spin lock and PD-CPMG experiment using 4 kHz DIPSI-2 decoupling produce a similar amount of error, which is not necessarily negligible (orange and red curves, respectively). One should be mindful of this effect when conducting measurements under somewhat extreme conditions where k_{ex} exceeds several tens of s^{-1}. In this situation it may be advisable to collect the data using higher decoupling power, which helps to eliminate the contribution from solvent exchange into R_2^{app}. For example, we have successfully recorded PD-CPMG experiment with 6 kHz DIPSI-2 decoupling and τ_{rel} extending to 640 ms (data not shown). Under certain circumstances one may also want to collect the data at

[5] In this expression $\tau_{ex} = k_{ex}^{-1}$ and ν_1 is the strength of the spin-lock.

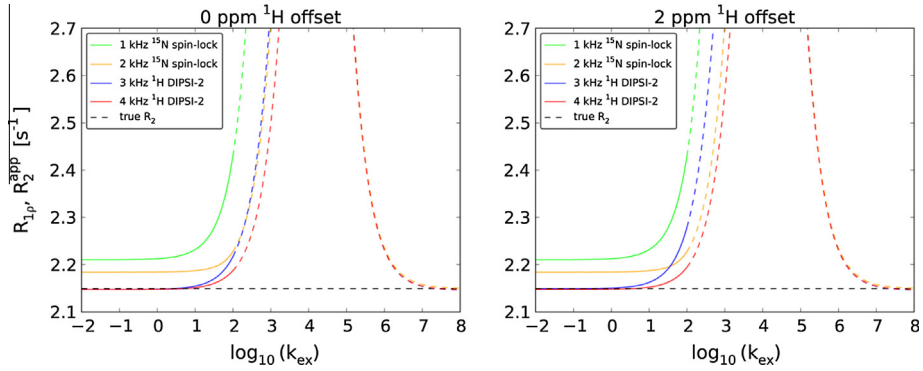

Fig. 10. Dependence of $R_{1\rho}$ and R_2^{app} rates from ^{15}N spin-lock and PD-CPMG experiments on solvent exchange rate k_{ex}. The dependence arises from the loss of $^1H^N$–^{15}N spin correlations due to amide solvent exchange. The simulations have been conducted using the same model as in Fig. 8, with $\nu_{off}^N = 0$. Solid lines correspond to the conditions of practical interest; black dashed horizontal line represents the true value of R_2. k_{ex} is given in the units of s^{-1}.

two decoupling field strengths, 3 and 4 kHz, to identify the rates affected by solvent exchange.

The range $k_{ex} \sim 10$–$100\ s^{-1}$ is relevant for IDPs under physiological conditions [74]. This is also the range where ^{15}N relaxation can be measured using the standard HSQC-based schemes. The remaining portion of Fig. 10, corresponding to ultra-fast solvent exchange, is mainly of academic interest (although suitable experimental schemes have also been developed [75,76]). The scalar contribution into $R_{1\rho}$ and R_2^{app} reaches several s^{-1} when exchange rate increases to ca. $10{,}000\ s^{-1}$ (the simulated data fall outside the area of the plot). With further increase in k_{ex} the scalar relaxation declines. This phenomenon is known as self-decoupling; in principle, self-decoupling leads to complete suppression of $^1J_{NH}$ evolution and allows for extraction of accurate R_2 rates (all profiles in the plot converge to the dashed horizontal line). For spin-lock experiment, the numeric results shown in Fig. 10 are in quantitative agreement with the calculations using Redfield-theory formula for scalar relaxation [73].

3.7. Sample heating

Sample heating is a potential concern in all heteronuclear spin–spin relaxation experiments as they deposit a copious amount of *rf* power into the sample. This is also true for the PD-CPMG scheme where proton decoupling is applied for a lengthy period of time, up to 0.5–1.0 s. The problem is exacerbated for samples with high conductivity. When using a sample of ubiquitin with pH 2.0 and recording PD-CPMG experiment with 6 kHz DIPSI-2 decoupling, we have observed heating-related artefacts such as characteristically distorted peak shapes [77]. This is attributable to the high content of H^+ ions in acidic solution; the problem disappears in the pH 3.0 sample (see below).

To mitigate the effect of heating, we have programmed the pulse sequence Fig. 2 in an interleaved fashion. In our scheme t_1 incrementation is controlled by an outer loop, whereas the array of τ_{rel} is parsed by an inner loop, alternating between short and long delays (e.g. 0, 560, 112, 448, 224, and 336 ms in the case of ubiquitin measurements). In this manner the degree of heating remains near-constant throughout the experiment. If necessary, the interleaved scheme can be further improved as described by Orekhov and co-workers [78]. The heat-equalizing element [77] can also be included into the sequence.

With the experimental setup used in our study it is straightforward to monitor the change in temperature during the PD-CPMG experiment. Toward this goal we have prepared a buffer solution of 8 M urea in D_2O, pH 3.0, which imitates ubiquitin sample. This solution was placed into NMR tube while the coaxial insert was filled with methanol. The original pulse sequence was then modified such as to allow for observation of the methanol ^{1}H spectrum (see Materials & Methods for details). This sequence was used to record a dataset which was equivalent to the original PD-CPMG in every way, except that each FID contained a strong methanol signal. The FIDs pertaining to the same τ_{rel} value have been added together, and the resulting methanol spectrum was used to determine the effective temperature associated with this particular τ_{rel} [79]. The results of this procedure are presented in Fig. 11.

Fig. 11 demonstrates that the sample heating in PD-CPMG experiment is close to uniform, as desired. In the absence of any *rf* pulsing, the temperature of the sample is determined to be 37.0 °C. The application of PD-CPMG sequence with 4 kHz DIPSI-2 decoupling and 2 s recycling delay raises the temperature to between 37.4 and 37.5 °C (green circles in the plot). When proton decoupling power is lowered to 3 kHz, the temperature is stabilized just under 37.4 °C (red circles). This is comparable to the spin-lock experiment employing τ_{rel} from 5 to 140 ms, where the similar interleaved setup heats the sample to slightly more than 37.3 °C (blue circles).

How significant is this level of heating? The data on ^{15}N R_2 relaxation in denatured ubiquitin are available at several different temperatures ([80,81], this work). From these data one can readily estimate that the temperature dependence of nitrogen R_2 is ca. $0.1\ s^{-1}/°C$. For the experiment at hand the increase in temperature amounts to ca. 0.4–0.5 °C, which translates into approximately 2% bias in the measured relaxation rates. While this amount of error may be tolerable, it can as well be eliminated by adjusting the setting of variable-temperature unit (in our case, to 36.5–36.6 °C).

Note the results illustrated in Fig. 11 pertain to the sample with moderately high conductivity. In contrast, for the sample in low conductivity buffer (α-spc SH3) the heating generated by spin-lock experiment is only 0.1 °C. For the same sample the PD-CPMG experiment employing 4 kHz DIPSI-2 decoupling and τ_{rel} delays as long as 843 ms produces only 0.2 °C heating.

4. General discussion and concluding remarks

The concepts used in our PD-CPMG experiment are similar to those previously used in the context of relaxation dispersion measurements [50,82]. In particular, Hansen et al. developed a constant-time CW-CPMG experiment where the loss of the signal is measured as a function of n_{tot}^{180}, the total number of 180° ^{15}N pulses. The use of the proton decoupling allows one to focus on the in-phase coherence N_x which has more favorable relaxation properties than the combination of N_x and $2N_yH_z$ previously used in the context of relaxation-compensated CPMG experiment [83]. The

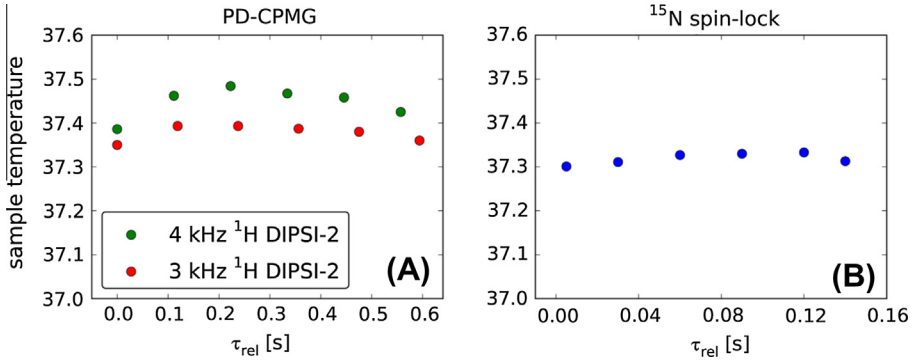

Fig. 11. True temperature associated with different τ_{rel} values as sampled by the PD-CPMG and spin-lock experiments (denatured ubiquitin, 8 M urea, pH 3.0). The same amount of heating is generated when one uses the sample with neutral pH and 50 mM NaCl.

new scheme can also be employed with a smaller number of pulses n_{tot}^{180}, which improves the sampling of relaxation dispersion profiles at low frequency ν_1^{CPMG}. As it should become clear from this brief discussion, the objectives of CW-CPMG experiment are quite different from what is described in this paper, and the technical details are different as well. In fact, it would be difficult to adapt CW-CPMG for the purpose of ^{15}N R_2 measurements since this sequence uses a continuous-wave proton decoupling with a relatively high level of power, 15 kHz.

The new proton-decoupled CPMG experiment has been developed with the goal to improve the precision of ^{15}N R_2 measurements in intrinsically disordered proteins at or near physiological conditions. However, the test measurements described in this paper only partially satisfy these conditions. While ubiquitin data have been collected at 37 °C, the sample was chemically denatured by application of 8 M urea, the pH was 3.0, and no particular attention has been paid to the ionic strength of the solution. How will our experiment fare if the measurements are conducted under more physiologically relevant conditions?

At 37 °C, pH 7.4 amide solvent exchange presents a potentially grave problem. Under these conditions, the exchange rates in disordered proteins mostly fall in the range 20–200 s^{-1} [74], causing significant line broadening and potentially compromising the accuracy of relaxation measurements. Although PD-CPMG measurements under these conditions should be possible, they will be extremely demanding. In this situation it may be advisable to lower pH to 7.0, as this value remains relevant for cytosol [84]. Given that histidine side chains in IDPs titrate near pH 6.0 [85], it should be possible to lower the pH without significantly altering the charges on the protein.

The ion content of the cytosol is typically assumed to be equivalent to 150 mM NaCl. We executed the PD-CPMG experiment on a sample containing this amount of salt and found that the temperature of the sample increased by 1.3 °C. This amount of heating is tolerable and does not affect the appearance of the spectra (verified experimentally). The increase in temperature can be compensated by adjusting the setting of the VT unit. We conclude that PD-CPMG measurements can be conducted using the samples with physiologically relevant salt concentrations.

Finally, let us consider solvent viscosity and the effect of co-solvents. The inside of the cells is known to be crowded, which causes substantial increases in ^{15}N R_2 rates [86]. Similarly, in our ubiquitin measurements the presence of 8 M urea led to elevated R_2 values, both through increased solvent viscosity and coordination of urea to the unfolded protein [87]. In contrast, NMR samples of IDPs are usually prepared without crowding agents or osmolytes. The ^{15}N R_2 rates in such samples are typically found to be 2–3 s^{-1} at the temperatures 15–20 °C [88–90], which corresponds to R_2 of ca. 1 s^{-1} at our target temperature 37 °C. For relaxation decay that is so slow, the advantages of the proposed PD-CPMG scheme should be even more significant. In other words, one may expect gains in precision that would surpass the factor of 3 found in this study.

The issue of precision can be critical for ^{15}N relaxation measurements in IDPs. Because of the propensity to aggregate and precipitate, the samples of IDPs often need to be prepared with low protein concentration, in the range of 10–100 μM. Furthermore, the measurement time is often limited to 1–10 h because the samples tend to quickly deteriorate. Solvent exchange further compounds to the problem, causing line-broadening in the already crowded spectra and further lowering signal-to-noise ratio. Under such circumstances it can be difficult to obtain high-quality data. At the same time it is very important that the data are precise. Indeed, ^{15}N relaxation measurements in IDPs typically pursue the effects that are subtle in nature. For instance, this may be a tenuous α-helical propensity which distinguishes physiologically relevant IDP from a random-coil-like peptide chain or a putative local cluster which is formed in response to a certain point mutation. In each case we rely on small changes in ^{15}N R_2 rates to pinpoint the effect of interest. Thus we are faced with the situation where it is essential, but at the same time very difficult, to collect high-precision ^{15}N R_2 data. The new PD-CPMG experiment is expected to be quite helpful in this regard.

The accuracy of the new experiment has been established through comparison with well-established $R_{1\rho}$ scheme. Such comparison was carried out for both unfolded and folded protein samples. We have determined that PD-CPMG experiment has a number of favorable properties. First, it records pure in-phase evolution during t_1 period and therefore offers an advantage in sensitivity and resolution. The signal-to-noise ratio in the PD-CPMG spectra of α-spc SH3 and ubiquitin are ca. 15% higher than in the comparable $R_{1\rho}$ spectra. This advantage becomes dramatic for proteins or peptides experiencing significant solvent exchange. Second, PD-CPMG data can be easily corrected for ^{15}N offset effect. In fact, this correction is small and can even be neglected, thus obviating the need for companion R_1 experiment. Third, the experiment is designed in such a way that solvent exchange does not interfere with the measurements. We avoid adding D_2O to the sample and maintain the constant degree of water saturation. The contribution from scalar relaxation of the second kind arising from solvent exchange remains minimal. Fourth, the experiment is highly stable with regard to pulse miscalibration and *rf* field inhomogeneity. The amount of sample heating is on par with the $R_{1\rho}$ measurements. Fifth, possible R_{ex} contributions into ^{15}N R_2 rates, which may arise from transient oligomerization or other potentially interesting effects, are largely retained in the PD-CPMG experiment because of the low ν_1^{CPMG}. This is arguably preferable to the standard measurement schemes where the application of strong spin-lock field or

frequent ^{15}N 180° pulses leads to partial suppression of R_{ex}. Sixth, PD-CPMG experiment has been adapted to probe $^{15}N^{\varepsilon}$ spins in Arg side chains which are likely to be a valuable target for future studies of protein internal dynamics. We have also verified that PD-CPMG sequence can be employed with ^{13}C-labeled samples using the setting $2\tau_{CP}\sim$5–10 ms (to be reported elsewhere). All of these attractive properties make us believe that PD-CPMG ^{15}N R_2 experiment will become a valuable addition to the arsenal of NMR experiments targeted at intrinsically disordered proteins.

5. Materials and methods

5.1. Protein samples

SH3 domain from chicken α-spectrin and human ubiquitin have been expressed in ^{15}N enriched M9 media and purified as described previously [91,92]. Protein concentrations were determined using UV absorbance at 280 nm. The sample of 1.5 mM α-spc SH3 has been prepared in H_2O, 20 mM citrate, 0.02% NaN_3, pH 3.5. The sample of 2.0 mM unfolded ubiquitin was prepared in H_2O, 8 M urea, pH 3.0. Two additional ubiquitin samples were prepared with protein concentration 50 and 100 μM. Sample volume in each case was 500 μL, with 100 μL of D_2O added into the coaxial insert of the NMR tube (Wilmad, WGS-5BL) to serve as external lock.

5.2. NMR spectroscopy

All NMR experiments were performed on Varian Inova-600 spectrometer equipped with triple-resonance z-axis gradient probe. The measurements were carried out at 25 °C for α-spc SH3 and 37 °C for unfolded ubiquitin. The backbone amide spectra were recorded with ^{15}N carrier at 119 ppm and ^{15}N spectral width of 30 ppm (α-spc SH3) or 22 ppm (ubiquitin). The data were collected with 64 t_1 increments and 1800 points in t_2 domain. The spectra of Arg ($^1H^{\varepsilon}$,$^{15}N^{\varepsilon}$) in α-spc SH3 were recorded with ^{15}N carrier as 85 ppm, ^{15}N spectral width of 10 ppm, and 16 t_1 increments. All data were collected with 4 scans per t_1 increment. The spectra were processed using NMRPipe [93]. Squared phase-shifted sine-bell window function was applied in both dimensions and the spectra were zero-filled to the size 4096×512 ($^1H^N$,^{15}N) or 4096×256 ($^1H^{\varepsilon}$,$^{15}N^{\varepsilon}$).

To ensure a clean comparison between PD-CPMG and spin-lock experiments, we have amended the standard $R_{1\rho}$ sequence [10] by adding a water-crusher element (red box on the right side of Fig. 2). In the spin-lock experiment we have used the following τ_{rel} delays: 5(1), 30(1), 60(2), 90(3), 120(4), and 140(4) ms (shown in brackets is the number of ^{1}H 180° pulses used to suppress dipolar-CSA cross-correlations). The ^{15}N spin-lock has been applied with *rf* field strength 1.7 kHz. All other experimental settings were the same as in PD-CPMG experiment, including the recycling delay d_1 = 2 s. ^{15}N R_1 data have also been recorded in order to determine ^{15}N offset correction for both $R_{1\rho}$ and PD-CPMG data (cf. Eq. (1)).

The spectra were integrated using the autoFit/nlinLS routines from the NMRPipe package. These routines operate on the entire "stack" of spectral planes, making an assumption that the peak position and the linewidths do not change significantly from one plane to the other and hence can be fitted in a global sense. This approach is especially helpful for quantitation of the weak peaks. The data were fitted assuming Gaussian peak shapes, as appropriate for the squared sine-bell apodization. The spectral assignments of α-spc SH3 and denatured ubiquitin were obtained from the previous reports [94,95].

To monitor sample temperature during the PD-CPMG experiment we have developed a special scheme based on the pulse sequence Fig. 2. Specifically, we changed the original sequence beginning with the acquisition period. Starting from this point the modified sequence reads: $g_{11} - \tau_{blank} - p_{H(90)} - t_2 - d_1$. Here g_{11} is the clean-up gradient with the strength 20 G/cm and duration 3.5 ms, τ_{blank} is 100 ms delay during which time the ^{15}N WALTZ-16 decoupling is turned on, $p_{H(90)}$ is hard proton pulse with the same phase as the receiver, t_2 is the acquisition period of 0.5 s, and d_1 is the recycling delay of 1.5 s. The purpose of this sequence is to record 1D spectrum of methanol (which is contained in the NMR tube coaxial insert) under the conditions that emulate the actual PD-CPMG measurement. We recommend using this accessory experiment when working with high conductivity (high ionic strength) samples, provided that accurate absolute values of R_2 are of interest.

5.3. Numerical simulations

We have simulated spin evolution of the two-spin ($^1H^N$, ^{15}N) and three-spin ($^1H^N$, ^{15}N and $^1H^{\alpha}$) systems during the τ_{rel} period of the PD-CPMG and spin-lock experiments. Taken into consideration were all sources of coherent evolution: *rf* fields, frequency offsets, and scalar couplings. In addition, Redfield matrix has been generated by rigorously including dipolar and CSA contributions. In the 2-spin simulations we have also included the "external" $^1H^{\alpha}$ spin, which manifested itself through dipolar contribution into the auto-relaxation rates of ($^1H^N$, ^{15}N) spin modes. In the 3-spin simulations, $^1H^{\alpha}$ was treated as a part of the spin system. We have assumed that $^3J_{HNH\alpha}$ = 10 Hz, $^2J_{N\alpha}$ = 5 Hz which is the upper limit for the respective experimentally observed couplings [96,97]. ^{15}N and $^1H^N$ CSA tensors were modeled according to the literature data [8,98]; $^1H^{\alpha}$ CSA tensor was assumed to be zero. The distance between $^1H^N$ and $^1H^{\alpha}$ was set to 1.84 Å. In order to emphasize the effect of dipole–dipolar cross-correlations, the angle between ^{15}N–$^1H^N$ and $^1H^N$–$^1H^{\alpha}$ vectors was set to zero. All simulations used a simple form of Lipari-Szabo spectral density [99], where it was assumed that τ_C = 2 ns, S^2 = 0.5, and τ_{fast} = 0. This parameterization is consistent with the previous analyses of ^{15}N relaxation in denatured protein [100] and correctly reproduces typical R_1 and R_2 values observed in denatured ubiquitin at 37 °C (Fig. 3b). *Rf* pulses were simulated with finite length. To model the effect of *rf* field inhomogeneity, the simulations were repeated for 100 discrete values of *rf* field strength uniformly distributed in the interval $[\nu_1 - 2\sigma, \nu_1 + 2\sigma]$. The signal intensity was then calculated as a weighted average of the results from multiple simulations. Solvent exchange was modeled as described previously [49]. Specifically, we recognize that any multi-spin mode combining ^{15}N and $^1H^N$ spin operators undergoes exchange-induced decay with the rate k_{ex}.

The simulations featuring 15×15 and 63×63 propagator matrices were repeated for the same set of τ_{rel} delays as used experimentally. The simulated signal intensities were then fitted with a single exponential, yielding the values of $R_{1\rho}$ or R_2^{app}. The results from 2- and 3-spin simulations proved to be virtually identical. This is not surprising considering that: (i) DIPSI-2 sequence has been designed to perform well in the presence of homonuclear couplings, such as $^3J_{HNH\alpha}$, (ii) the train of ^{15}N 180° CPMG pulses is sufficient to eliminate the effect of the small $^2J_{NH\alpha}$ coupling, with off-resonance DIPSI-2 providing additional insurance, and (iii) three-spin modes generated by dipole–dipolar cross-correlations are effectively dephased by DIPSI-2 decoupling.

Acknowledgment

This study was supported by the funds from NSF Grant MCB 1158347.

References

[1] M.E. Hodsdon, D.P. Cistola, Ligand binding alters the backbone mobility of intestinal fatty acid-binding protein as monitored by ^{15}N NMR relaxation and ^{1}H exchange, Biochemistry 36 (1997) 2278–2290.

[2] L. Zidek, M.V. Novotny, M.J. Stone, Increased protein backbone conformational entropy upon hydrophobic ligand binding, Nat. Struct. Biol. 6 (1999) 1118–1121.

[3] M.J. Seewald, K. Pichumani, C. Stowell, B.V. Tibbals, L. Regan, M.J. Stone, The role of backbone conformational heat capacity in protein stability: temperature-dependent dynamics of the B1 domain of Streptococcal protein G, Protein Sci. 9 (2000) 1177–1193.

[4] J.M. Vinther, S.M. Kristensen, J.J. Led, Enhanced stability of a protein with increasing temperature, J. Am. Chem. Soc. 133 (2011) 271–278.

[5] L. Ragona, M. Catalano, M. Luppi, D. Cicero, T. Eliseo, J. Foote, F. Fogolari, L. Zetta, H. Molinari, NMR dynamic studies suggest that allosteric activation regulates ligand binding in chicken liver bile acid-binding protein, J. Biol. Chem. 281 (2006) 9697–9709.

[6] R. Das, M.T. Mazhab-Jafari, S. Chowdhury, S. SilDas, R. Selvaratnam, G. Melacini, Entropy-driven cAMP-dependent allosteric control of inhibitory interactions in exchange proteins directly activated by cAMP, J. Biol. Chem. 283 (2008) 19691–19703.

[7] L.S. Yao, B. Vögeli, J.F. Ying, A. Bax, NMR determination of amide N-H equilibrium bond length from concerted dipolar coupling measurements, J. Am. Chem. Soc. 130 (2008) 16518–16520.

[8] L.S. Yao, A. Grishaev, G. Cornilescu, A. Bax, Site-specific backbone amide ^{15}N chemical shift anisotropy tensors in a small protein from liquid crystal and cross-correlated relaxation measurements, J. Am. Chem. Soc. 132 (2010) 4295–4309.

[9] D.F. Hansen, H.Q. Feng, Z. Zhou, Y.W. Bai, L.E. Kay, Selective characterization of microsecond motions in proteins by NMR relaxation, J. Am. Chem. Soc. 131 (2009) 16257–16265.

[10] D.M. Korzhnev, N.R. Skrynnikov, O. Millet, D.A. Torchia, L.E. Kay, An NMR experiment for the accurate measurement of heteronuclear spin-lock relaxation rates, J. Am. Chem. Soc. 124 (2002) 10743–10753.

[11] F. Ferrage, D. Cowburn, R. Ghose, Accurate sampling of high-frequency motions in proteins by steady-state ^{15}N-{^{1}H} nuclear Overhauser effect measurements in the presence of cross-correlated relaxation, J. Am. Chem. Soc. 131 (2009) 6048–6049.

[12] S. Jurt, O. Zerbe, A study on the influence of fast amide exchange on the accuracy of ^{15}N relaxation rate constants, J. Biomol. NMR 54 (2012) 389–400.

[13] A.M. Mandel, M. Akke, A.G. Palmer, Backbone dynamics of Escherichia coli ribonuclease HI: correlations with structure and function in an active enzyme, J. Mol. Biol. 246 (1995) 144–163.

[14] M. Andrec, G.T. Montelione, R.M. Levy, Estimation of dynamic parameters from NMR relaxation data using the Lipari-Szabo model-free approach and Bayesian statistical methods, J. Magn. Reson. 139 (1999) 408–421.

[15] R. Cole, J.P. Loria, FAST-Modelfree: a program for rapid automated analysis of solution NMR spin-relaxation data, J. Biomol. NMR 26 (2003) 203–213.

[16] D.Q. Jin, M. Andrec, G.T. Montelione, R.M. Levy, Propagation of experimental uncertainties using the Lipari-Szabo model-free analysis of protein dynamics, J. Biomol. NMR 12 (1998) 471–492.

[17] E.J. d'Auvergne, P.R. Gooley, The use of model selection in the model-free analysis of protein dynamics, J. Biomol. NMR 25 (2003) 25–39.

[18] J.H. Chen, C.L. Brooks, P.E. Wright, Model-free analysis of protein dynamics: assessment of accuracy and model selection protocols based on molecular dynamics simulation, J. Biomol. NMR 29 (2004) 243–257.

[19] J.M. Schurr, H.P. Babcock, B.S. Fujimoto, A test of the model-free formulas. Effects of anisotropic rotational diffusion and dimerization, J. Magn. Reson. Ser. B 105 (1994) 211–224.

[20] N. Tjandra, S.E. Feller, R.W. Pastor, A. Bax, Rotational diffusion anisotropy of human ubiquitin from ^{15}N NMR relaxation, J. Am. Chem. Soc. 117 (1995) 12562–12566.

[21] L.K. Lee, M. Rance, W.J. Chazin, A.G. Palmer, Rotational diffusion anisotropy of proteins from simultaneous analysis of ^{15}N and ^{13}C$^{\alpha}$ nuclear spin relaxation, J. Biomol. NMR 9 (1997) 287–298.

[22] P. Dosset, J.C. Hus, M. Blackledge, D. Marion, Efficient analysis of macromolecular rotational diffusion from heteronuclear relaxation data, J. Biomol. NMR 16 (2000) 23–28.

[23] A.L. Lee, A.J. Wand, Assessing potential bias in the determination of rotational correlation times of proteins by NMR relaxation, J. Biomol. NMR 13 (1999) 101–112.

[24] S.L. Chang, N. Tjandra, Temperature dependence of protein backbone motion from carbonyl ^{13}C and amide ^{15}N NMR relaxation, J. Magn. Reson. 174 (2005) 43–53.

[25] S.A. Showalter, R. Brüschweiler, Validation of molecular dynamics simulations of biomolecules using NMR spin relaxation as benchmarks: application to the AMBER99SB force field, J. Chem. Theory Comput. 3 (2007) 961–975.

[26] S. Mine, S. Tate, T. Ueda, M. Kainosho, T. Imoto, Analysis of the relationship between enzyme activity and its internal motion using nuclear magnetic resonance: ^{15}N relaxation studies of wild-type and mutant lysozyme, J. Mol. Biol. 286 (1999) 1547–1565.

[27] B.F. Volkman, D. Lipson, D.E. Wemmer, D. Kern, Two-state allosteric behavior in a single-domain signaling protein, Science 291 (2001) 2429–2433.

[28] S.W. Homans, Probing the binding entropy of ligand-protein interactions by NMR, ChemBioChem 6 (2005) 1585–1591.

[29] S.R. Tzeng, C.G. Kalodimos, Protein activity regulation by conformational entropy, Nature 488 (2012) 236–240.

[30] A.K. Dunker, C.J. Oldfield, J.W. Meng, P. Romero, J.Y. Yang, J.W. Chen, V. Vacic, Z. Obradovic, V.N. Uversky, The unfoldomics decade: an update on intrinsically disordered proteins, BMC Genomics 9 (S2) (2008) S1.

[31] A.B. Sigalov, A.V. Zhuravleva, V.Y. Orekhov, Binding of intrinsically disordered proteins is not necessarily accompanied by a structural transition to a folded form, Biochimie 89 (2007) 419–421.

[32] J. Song, L.W. Guo, H. Muradov, N.O. Artemyev, A.E. Ruoho, J.L. Markley, Intrinsically disordered gamma-subunit of cGMP phosphodiesterase encodes functionally relevant transient secondary and tertiary structure, Proc. Natl. Acad. Sci. U. S. A 105 (2008) 1505–1510.

[33] M.D. Mukrasch, S. Bibow, J. Korukottu, S. Jeganathan, J. Biernat, C. Griesinger, E. Mandelkow, M. Zweckstetter, Structural polymorphism of 441-residue Tau at single residue resolution, PLoS Biol. 7 (2009) 399–414.

[34] J.A. Jones, P. Hodgkinson, A.L. Barker, P.J. Hore, Optimal sampling strategies for the measurement of spin-spin relaxation times, J. Magn. Reson. Ser. B 113 (1996) 25–34.

[35] P.A. Keifer, 90° degrees pulse width calibrations: how to read a pulse width array, Concept Magn. Reson. 11 (1999) 165–180.

[36] D. Ban, A.D. Gossert, K. Giller, S. Becker, C. Griesinger, D. Lee, Exceeding the limit of dynamics studies on biomolecules using high spin-lock field strengths with a cryogenically cooled probehead, J. Magn. Reson. 221 (2012) 1–4.

[37] F. Massi, E. Johnson, C.Y. Wang, M. Rance, A.G. Palmer, NMR R_{1r} rotating-frame relaxation with weak radio frequency fields, J. Am. Chem. Soc. 126 (2004) 2247–2256.

[38] A.G. Palmer, N.J. Skelton, W.J. Chazin, P.E. Wright, M. Rance, Suppression of the effects of cross-correlation between dipolar and anisotropic chemical shift relaxation mechanisms in the measurement of spin spin relaxation rates, Mol. Phys. 75 (1992) 699–711.

[39] S. Zinn-Justin, P. Berthault, M. Guenneugues, H. Desvaux, Off-resonance rf fields in heteronuclear NMR: application to the study of slow motions, J. Biomol. NMR 10 (1997) 363–372.

[40] Y. Pang, M. Buck, E.R.P. Zuiderweg, Backbone dynamics of the ribonuclease binase active site area using multinuclear (^{15}N and ^{13}CO) NMR relaxation and computational molecular dynamics, Biochemistry 41 (2002) 2655–2666.

[41] W. Myint, Q.G. Gong, R. Ishima, Practical aspects of ^{15}N CPMG transverse relaxation experiments for proteins in solution, Concept Magn. Reson. A 34A (2009) 63–75.

[42] G.N.B. Yip, E.R.P. Zuiderweg, A phase cycle scheme that significantly suppresses offset-dependent artifacts in the R_2-CPMG ^{15}N relaxation experiment, J. Magn. Reson. 171 (2004) 25–36.

[43] D. Long, M.L. Liu, D.W. Yang, Accurately probing slow motions on millisecond timescales with a robust NMR relaxation experiment, J. Am. Chem. Soc. 130 (2008) 2432–2433.

[44] A.D. Bain, C.K. Anand, Z.H. Nie, Exact solution of the CPMG pulse sequence with phase variation down the echo train: application to R_2 measurements, J. Magn. Reson. 209 (2011) 183–194.

[45] W. Myint, Y.F. Cai, C.A. Schiffer, R. Ishima, Quantitative comparison of errors in ^{15}N transverse relaxation rates measured using various CPMG phasing schemes, J. Biomol. NMR 53 (2012) 13–23.

[46] A.J. Shaka, C.J. Lee, A. Pines, Iterative schemes for bilinear operators: application to spin decoupling, J. Magn. Reson. 77 (1988) 274–293.

[47] A. Bax, M. Ikura, L.E. Kay, D.A. Torchia, R. Tschudin, Comparison of different modes of two-dimensional reverse-correlation NMR for the study of proteins, J. Magn. Reson. 86 (1990) 304–318.

[48] T.J. Norwood, J. Boyd, J.E. Heritage, N. Soffe, I.D. Campbell, Comparison of techniques for ^{1}H-detected heteronuclear ^{1}H–^{15}N spectroscopy, J. Magn. Reson. 87 (1990) 488–501.

[49] N.R. Skrynnikov, R.R. Ernst, Detection of intermolecular chemical exchange through decorrelation of two-spin order, J. Magn. Reson. 137 (1999) 276–280.

[50] D.F. Hansen, P. Vallurupalli, L.E. Kay, An improved ^{15}N relaxation dispersion experiment for the measurement of millisecond time-scale dynamics in proteins, J. Phys. Chem. B 112 (2008) 5898–5904.

[51] B.A. Messerle, G. Wider, G. Otting, C. Weber, K. Wüthrich, Solvent suppression using a spin lock in 2D and 3D NMR spectroscopy with H_2O solutions, J. Magn. Reson. 85 (1989) 608–613.

[52] L.E. Kay, P. Keifer, T. Saarinen, Pure absorption gradient enhanced heteronuclear single quantum correlation spectroscopy with improved sensitivity, J. Am. Chem. Soc. 114 (1992) 10663–10665.

[53] J. Schleucher, M. Sattler, C. Griesinger, Coherence selection by gradients without signal attenuation: application to the 3-dimensional HNCO experiment, Angew. Chem.-Int. Ed. Engl. 32 (1993) 1489–1491.

[54] D. Marion, M. Ikura, R. Tschudin, A. Bax, Rapid recording of 2D NMR spectra without phase cycling: application to the study of hydrogen exchange in proteins, J. Magn. Reson. 85 (1989) 393–399.

[55] E. Kupce, J. Boyd, I.D. Campbell, Short selective pulses for biochemical applications, J. Magn. Reson. Ser. B 106 (1995) 300–303.

[56] H. Geen, R. Freeman, Band-selective radiofrequency pulses, J. Magn. Reson. 93 (1991) 93–141.

[57] S. Grzesiek, A. Bax, The importance of not saturating H_2O in Protein NMR: application to sensitivity enhancement and NOE measurements, J. Am. Chem. Soc. 115 (1993) 12593–12594.

[58] N.A. Farrow, R. Muhandiram, A.U. Singer, S.M. Pascal, C.M. Kay, G. Gish, S.E. Shoelson, T. Pawson, J.D. Forman-Kay, L.E. Kay, Backbone dynamics of a free and a phosphopeptide-complexed src homology 2 domain studied by ^{15}N NMR relaxation, Biochemistry 33 (1994) 5984–6003.
[59] K. Chen, N. Tjandra, Water proton spin saturation affects measured protein backbone ^{15}N spin relaxation rates, J. Magn. Reson. 213 (2011) 151–157.
[60] N.A. Lakomek, J.F. Ying, A. Bax, Measurement of ^{15}N relaxation rates in perdeuterated proteins by TROSY-based methods, J. Biomol. NMR 53 (2012) 209–221.
[61] A.E. Kelly, H.D. Ou, R. Withers, V. Dotsch, Low-conductivity buffers for high-sensitivity NMR measurements, J. Am. Chem. Soc. 124 (2002) 12013–12019.
[62] F. Lohr, H. Ruterjans, Detection of nitrogen-nitrogen J-couplings in proteins, J. Magn. Reson. 132 (1998) 130–137.
[63] R. Ishima, D.A. Torchia, Extending the range of amide proton relaxation dispersion experiments in proteins using a constant-time relaxation-compensated CPMG approach, J. Biomol. NMR 25 (2003) 243–248.
[64] A.L. Hansen, P. Lundstrom, A. Velyvis, L.E. Kay, Quantifying millisecond exchange dynamics in proteins by CPMG relaxation dispersion NMR using side-chain ^{1}H probes, J. Am. Chem. Soc. 134 (2012) 3178–3189.
[65] D.M. Korzhnev, E.V. Tischenko, A.S. Arseniev, Off-resonance effects in ^{15}N T_2 CPMG measurements, J. Biomol. NMR 17 (2000) 231–237.
[66] G.S. Rule, T.K. Hitchens, Fundamentals of Protein NMR Spectroscopy, Springer, Netherlands, 2006.
[67] M. Kjaergaard, S. Brander, F.M. Poulsen, Random coil chemical shift for intrinsically disordered proteins: effects of temperature and pH, J. Biomol. NMR 49 (2011) 139–149.
[68] J. Iwahara, Y.S. Jung, G.M. Clore, Heteronuclear NMR spectroscopy for lysine NH3 groups in proteins: unique effect of water exchange on ^{15}N transverse relaxation, J. Am. Chem. Soc. 129 (2007) 2971–2980.
[69] B.S. Blaum, J.A. Deakin, C.M. Johansson, A.P. Herbert, P.N. Barlow, M. Lyon, D. Uhrin, Lysine and arginine side chains in glycosaminoglycan-protein complexes investigated by NMR, cross-linking, and mass spectrometry: a case study of the Factor H - Heparin interaction, J. Am. Chem. Soc. 132 (2010) 6374–6381.
[70] K. Hayamizu, W.S. Price, A new type of sample tube for reducing convection effects in PGSE-NMR measurements of self-diffusion coefficients of liquid samples, J. Magn. Reson. 167 (2004) 328–333.
[71] T. Yamazaki, S.M. Pascal, A.U. Singer, J.D. Forman-Kay, L.E. Kay, NMR pulse schemes for the sequence-specific assignment of arginine guanidino ^{15}N and ^{1}H chemical shifts in proteins, J. Am. Chem. Soc. 117 (1995) 3556–3564.
[72] J.C. Hindman, A. Svirmickas, M. Wood, Relaxation processes in water. A study of the proton spin-lattice relaxation time, J. Chem. Phys. 59 (1973) 1517–1522.
[73] A. Abragam, Principles of Nuclear Magnetism, Oxford University Press, USA, 1983.
[74] Y.W. Bai, J.S. Milne, L. Mayne, S.W. Englander, Primary structure effects on peptide group hydrogen exchange, Proteins: Struct., Funct., Genet. 17 (1993) 75–86.
[75] F. Kateb, P. Pelupessy, G. Bodenhausen, Measuring fast hydrogen exchange rates by NMR spectroscopy, J. Magn. Reson. 184 (2007) 108–113.
[76] P.R. Vasos, J.B. Hall, R. Kummerle, D. Fushman, Measurement of ^{15}N relaxation in deuterated amide groups in proteins using direct nitrogen detection, J. Biomol. NMR 36 (2006) 27–36.
[77] A.C. Wang, A. Bax, Minimizing the effects of radiofrequency heating in multidimensional NMR experiments, J. Biomol. NMR 3 (1993) 715–720.
[78] V.Y. Orekhov, D.M. Korzhnev, T. Diercks, H. Kessler, A.S. Arseniev, ^{1}H–^{15}N NMR dynamic study of an isolated alpha-helical peptide (1–36)-bacteriorhodopsin reveals the equilibrium helix-coil transitions, J. Biomol. NMR 14 (1999) 345–356.
[79] C. Ammann, P. Meier, A.E. Merbach, A simple multi-nuclear NMR thermometer, J. Magn. Reson. 46 (1982) 319–321.
[80] J. Wirmer, W. Peti, H. Schwalbe, Motional properties of unfolded ubiquitin: a model for a random coil protein, J. Biomol. NMR 35 (2006) 175–186.
[81] Y. Xue, N.R. Skrynnikov, Motion of a disordered polypeptide chain as studied by paramagnetic relaxation enhancements, ^{15}N relaxation, and Molecular Dynamics simulations: how fast is segmental diffusion in denatured ubiquitin?, J Am. Chem. Soc. 133 (2011) 14614–14628.
[82] S.M. Kristensen, G. Siegal, A. Sankar, P.C. Driscoll, Backbone dynamics of the C-terminal SH2 domain of the p85 alpha subunit of phosphoinositide 3-kinase: effect of phosphotyrosine-peptide binding and characterization of slow conformational exchange processes, J. Mol. Biol. 299 (2000) 771–788.
[83] J.P. Loria, M. Rance, A.G. Palmer, A relaxation-compensated Carr-Purcell-Meiboom-Gill sequence for characterizing chemical exchange by NMR spectroscopy, J. Am. Chem. Soc. 121 (1999) 2331–2332.
[84] R. Orij, J. Postmus, A. Ter Beek, S. Brul, G.J. Smits, In vivo measurement of cytosolic and mitochondrial pH using a pH-sensitive GFP derivative in Saccharomyces cerevisiae reveals a relation between intracellular pH and growth, Microbiology 155 (2009) 268–278.
[85] R.L. Croke, S.M. Patil, J. Quevreaux, D.A. Kendall, A.T. Alexandrescu, NMR determination of pK_a values in α-synuclein, Protein Sci. 20 (2011) 256–269.
[86] E.A. Cino, M. Karttunen, W.Y. Choy, Effects of molecular crowding on the dynamics of intrinsically disordered proteins, PLoS One 7 (2012) e49876.
[87] M. Candotti, S. Esteban-Martin, X. Salvatella, M. Orozco, Toward an atomistic description of the urea-denatured state of proteins, Proc. Natl. Acad. Sci. U. S. A 110 (2013) 5933–5938.
[88] M.K. Cho, G. Nodet, H.Y. Kim, M.R. Jensen, P. Bernado, C.O. Fernandez, S. Becker, M. Blackledge, M. Zweckstetter, Structural characterization of alpha-synuclein in an aggregation prone state, Protein Sci. 18 (2009) 1840–1846.
[89] R. Silvers, F. Sziegat, H. Tachibana, S. Segawa, S. Whittaker, U.L. Gunther, F. Gabel, J.R. Huang, M. Blackledge, J. Wirmer-Bartoschek, H. Schwalbe, Modulation of structure and dynamics by disulfide bond formation in unfolded states, J. Am. Chem. Soc. 134 (2012) 6846–6854.
[90] J. Roche, J. Ying, A.S. Maltsev, A. Bax, Impact of hydrostatic pressure on an intrinsically disordered protein: a high-pressure NMR study of α-synuclein, Chembiochem 14 (2013) 1754–1761.
[91] J. Pauli, B. van Rossum, H. Forster, H.J.M. de Groot, H. Oschkinat, Sample optimization and identification of signal patterns of amino acid side chains in 2D RFDR spectra of the α-spectrin SH3 domain, J. Magn. Reson. 143 (2000) 411–416.
[92] G.A. Lazar, J.R. Desjarlais, T.M. Handel, De novo design of the hydrophobic core of ubiquitin, Protein Sci. 6 (1997) 1167–1178.
[93] F. Delaglio, S. Grzesiek, G.W. Vuister, G. Zhu, J. Pfeifer, A. Bax, NMRPipe – a multidimensional spectral processing system based on unix pipes, J. Biomol. NMR 6 (1995) 277–293.
[94] F.J. Blanco, A.R. Ortiz, L. Serrano, ^{1}H and ^{15}N NMR assignment and solution structure of the SH3 domain of spectrin: comparison of unrefined and refined structure sets with the crystal structure, J. Biomol. NMR 9 (1997) 347–357.
[95] W. Peti, L.J. Smith, C. Redfield, H. Schwalbe, Chemical shifts in denatured proteins: Resonance assignments for denatured ubiquitin and comparisons with other denatured proteins, J. Biomol. NMR 19 (2001) 153–165.
[96] A.C. Wang, A. Bax, Reparameterization of the Karplus relation for $^{3}J(H^{\alpha}\text{-}N)$ and $^{3}J(H^{N}\text{-}C')$ in peptides from uniformly $^{13}C/^{15}N$-enriched human ubiquitin, J. Am. Chem. Soc. 117 (1995) 1810–1813.
[97] J.M. Schmidt, Y. Hua, F. Lohr, Correlation of ^{2}J couplings with protein secondary structure, Proteins 78 (2010) 1544–1562.
[98] M. Ottiger, N. Tjandra, A. Bax, Magnetic field dependent amide ^{15}N chemical shifts in a protein-DNA complex resulting from magnetic ordering in solution, J. Am. Chem. Soc. 119 (1997) 9825–9830.
[99] G. Lipari, A. Szabo, Model-free approach to the interpretation of nuclear magnetic resonance relaxation in macromolecules. 1. Theory and range of validity, J. Am. Chem. Soc. 104 (1982) 4546–4559.
[100] N.A. Farrow, O.W. Zhang, J.D. Forman-Kay, L.E. Kay, Characterization of the backbone dynamics of folded and denatured states of an SH3 domain, Biochemistry 36 (1997) 2390–2402.